Exact Spectral Gaps of the Asymmetric Exclusion Process with Open Boundaries

Jan de Gier[1] **and Fabian H L Essler** [2]

[1] ARC Centre of Excellence for Mathematics and Statistics of Complex Systems, Department of Mathematics and Statistics, The University of Melbourne, 3010 VIC, Australia
[2] Rudolf Peierls Centre for Theoretical Physics, University of Oxford, 1 Keble Road, Oxford, OX1 3NP, United Kingdom

Abstract. We derive the Bethe ansatz equations describing the complete spectrum of the transition matrix of the partially asymmetric exclusion process with the most general open boundary conditions. By analysing these equations in detail for the cases of totally asymmetric and symmetric diffusion, we calculate the finite-size scaling of the spectral gap, which characterizes the approach to stationarity at large times. In the totally asymmetric case we observe boundary induced crossovers between massive, diffusive and KPZ scaling regimes. We further study higher excitations, and demonstrate the absence of oscillatory behaviour at large times on the "coexistence line", which separates the massive low and high density phases. In the maximum current phase, oscillations are present on the KPZ scale $t \propto L^{-3/2}$. While independent of the boundary parameters, the spectral gap as well as the oscillation frequency in the maximum current phase have different values compared to the totally asymmetric exclusion process with periodic boundary conditions. We discuss a possible interpretation of our results in terms of an effective domain wall theory.
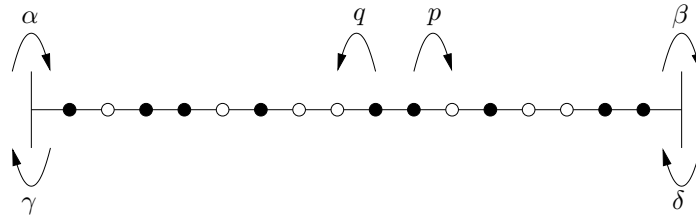
The partially asymmetric simple exclusion process (PASEP) [1, 2] is a model describing the asymmetric diffusion of hard-core particles along a one-dimensional chain with L sites. Over the last decade it has become one of the most studied models of non-equilibrium statistical mechanics, see [3, 4] for recent reviews. This is due to its close relationship to growth phenomena and the KPZ equation [5], its use as a microscopic model for driven diffusive systems [6] and shock formation [7], its applicability to molecular diffusion in zeolites [8], biopolymers [9–11], traffic flow [12] and other one-dimensional complex systems [13].

At large times the PASEP exhibits a relaxation towards a non-equilibrium stationary state. An interesting feature of the PASEP is the presence of boundary induced phase transitions [14]. In particular, in an open system with two boundaries at which particles are injected and extracted with given rates, the bulk behaviour in the stationary state is strongly dependent on the injection and extraction rates. Over the last decade many stationary state properties of the PASEP with open boundaries have been determined exactly [3, 4, 15, 16, 19–22].

On the other hand, much less is known about its dynamics. This is in contrast to the PASEP on a ring for which exact results using Bethe's ansatz have been available for a long time [23–25]. For open boundaries there have been several studies of dynamical properties based mainly on numerical and phenomenological methods [26–30]. Very recently a real-space renormalization group approach was introduced, which allows for the determination of the dynamical exponents [31].

In this work, elaborating on [32], we employ Bethe's ansatz to obtain exact results for the approach to stationarity at large times in the PASEP with open boundaries. Upon varying the boundary rates, we find crossovers in massive regions, with dynamic exponents $z = 0$, and between massive and scaling regions with diffusive ($z = 2$) and KPZ ($z = 3/2$) behaviour.

Figure 1. Transition rates for the partially asymmetric exclusion process.

The dynamical rules of the PASEP are as follows. At any given time t each site is either occupied by a particle or empty and the system evolves subject to the following rules. In the bulk of the system ($i = 2, \ldots, L-1$) a particle attempts to hop one site to the right with rate p and one site to the left with rate q. The hop is prohibited if the neighbouring site is occupied. On the first and last sites these rules are modified. If site $i = 1$ is empty, a particle may enter the system with rate α. If on the other hand site 1 is occupied by a particle, the latter will leave the system with rate γ. Similarly, at $i = L$ particles are injected and extracted with rates δ and β respectively.

With every site i we associate a Boolean variable τ_i, indicating whether a particle is present ($\tau_i = 1$) or not ($\tau_i = 0$). Let $|0\rangle$ and $|1\rangle$ denote the standard basis vectors in $\mathbb{C}^2$. A state of the system at time t is then characterized by the probability distribution

$$|P(t)\rangle = \sum_{\boldsymbol{\tau}} P(\boldsymbol{\tau}|t)|\boldsymbol{\tau}\rangle, \tag{0.1}$$

where

$$|\boldsymbol{\tau}\rangle = |\tau_1, \ldots, \tau_L\rangle = \bigotimes_{i=1}^{L} |\tau_i\rangle. \tag{0.2}$$

The time evolution of $|P(t)\rangle$ is governed by the aforementioned rules and as a result is subject to the master equation

$$\frac{\mathrm{d}}{\mathrm{d}t}|P(t)\rangle = M|P(t)\rangle, \tag{0.3}$$

where the PASEP transition matrix M consists of two-body interactions only and is given by

$$M = \sum_k I^{\otimes k-1} \otimes \widetilde{M} \otimes I^{\otimes L-k-1} + m_1 \otimes I^{\otimes L-1} + I^{\otimes L-1} \otimes m_L. \tag{0.4}$$

Here, I is the identity matrix on $\mathbb{C}^2$ and $\widetilde{M} : \mathbb{C}^2 \otimes \mathbb{C}^2 \to \mathbb{C}^2 \otimes \mathbb{C}^2$ is given by

$$\widetilde{M} = \begin{pmatrix} 0 & 0 & 0 & 0 \\ 0 & -q & p & 0 \\ 0 & q & -p & 0 \\ 0 & 0 & 0 & 0 \end{pmatrix}. \tag{0.5}$$

The boundary contributions m_1 and m_L describe injection (extraction) of particles with rates α and δ (γ and β) at sites 1 and L. In addition, as a tool to compute current fluctuations [33, 34], we introduce a fugacity e^λ conjugate to the current on the first site. The boundary contributions then are

$$m_1 = \begin{pmatrix} -\alpha & \gamma\mathrm{e}^{-\lambda} \\ \alpha\mathrm{e}^\lambda & -\gamma \end{pmatrix}, \qquad m_L = \begin{pmatrix} -\delta & \beta \\ \delta & -\beta \end{pmatrix}. \tag{0.6}$$

Strictly speaking, with the inclusion of λ the matrix M is no longer a transition matrix of a stochastic process. In the following however, we will still refer to M as the transition matrix of the PASEP also for nonzero values of λ.

At $\lambda = 0$, the matrix M has a unique stationary state corresponding to eigenvalue zero. For positive rates, all other eigenvalues of M have non-positive real parts. The large time behaviour of the PASEP is dominated by the eigenstates of M with the largest real parts of the corresponding eigenvalues. In the next sections we will determine the eigenvalues of M using Bethe's ansatz. The latter reduces the problem of determining the spectrum of M to solving a system of coupled polynomial equations of degree $3L-1$. Using these equations, the spectrum of M can be studied numerically for very large L, and, as we will show, analytic results can be obtained in the limit $L \to \infty$.

1. Relation to the spin-1/2 Heisenberg XXZ chain with open boundaries

It is well known that the transition matrix M is related to the Hamiltonian H of the open spin-1/2 XXZ quantum spin chain through a similarity transformation

$$M = -\sqrt{pq}\, U_\mu^{-1} H_{\mathrm{XXZ}} U_\mu, \tag{1.1}$$

where U_μ and H_{XXZ} are given by (see e.g. [19, 20]),

$$U_\mu = \bigotimes_{i=1}^{L} \begin{pmatrix} 1 & 0 \\ 0 & \mu Q^{j-1} \end{pmatrix}, \tag{1.2}$$

$$H_{\mathrm{XXZ}} = -\frac{1}{2} \sum_{j=1}^{L-1} \left[\sigma_j^{\mathrm{x}} \sigma_{j+1}^{\mathrm{x}} + \sigma_j^{\mathrm{y}} \sigma_{j+1}^{\mathrm{y}} - \Delta \sigma_j^{\mathrm{z}} \sigma_{j+1}^{\mathrm{z}} + h(\sigma_{j+1}^{\mathrm{z}} - \sigma_j^{\mathrm{z}}) + \Delta \right]$$
$$+ B_1 + B_L. \tag{1.3}$$

The parameters Δ and h, and the boundary terms B_1 and B_L are related to the PASEP transition rates by

$$B_1 = \frac{1}{2\sqrt{pq}} \left(\alpha + \gamma + (\alpha - \gamma)\sigma_1^{\mathrm{z}} - 2\alpha\mu \mathrm{e}^{\lambda}\sigma_1^- - 2\gamma\mu^{-1}\mathrm{e}^{-\lambda}\sigma_1^+ \right),$$

$$B_L = \frac{1}{2\sqrt{pq}} \left(\beta + \delta - (\beta - \delta)\sigma_L^{\mathrm{z}} - 2\delta\mu Q^{L-1}\sigma_L^- - 2\beta\mu^{-1}Q^{-L+1}\sigma_L^+ \right),$$

$$\Delta = -\frac{1}{2}(Q + Q^{-1}), \quad h = \frac{1}{2}(Q - Q^{-1}), \quad Q = \sqrt{\frac{q}{p}}. \tag{1.4}$$

Here σ_j^{x}, σ_j^{y} and σ_j^{z} are the usual Pauli matrices, $\sigma_j^{\pm} = (\sigma_j^{\mathrm{x}} \pm \mathrm{i}\sigma_j^{\mathrm{y}})/2$, and μ is a free gauge parameter on which the spectrum does not depend.

　　The expression in (1.3) is the Hamiltonian of the ferromagnetic $U_Q(SU(2))$ invariant quantum spin chain [35] with added boundary terms B_1 and B_L. We note that the boundary terms contain non-diagonal contributions ($\sigma_1^{\pm}$, $\sigma_L^{\pm}$) with L-dependent coefficients. In the absence of the boundary terms the spectrum of the Hamiltonian is massive, i.e. there is a finite gap between the absolute ground states and the lowest excited states. As is shown below, the boundary terms lead to the emergence of several different phases. Some of these phases exhibit a spectral gap in the limit $L \to \infty$ in the sense that there is a finite gap in the real part of the eigenvalue of the transition matrix. Other phases feature gapless excited states.

　　In order to make contact with the literature, we start by relating the PASEP parameters to those used in previous analyses of the spin-1/2 XXZ quantum spin chain with open boundaries. For the latter we employ notations similar to [36], in which the XXZ Hamiltonian reads (up to a constant shift in energy)

$$H = -\frac{1}{2} \sum_{i=1}^{L-1} \left[\sigma_i^x \sigma_{i+1}^x + \sigma_i^y \sigma_{i+1}^y - \cos\eta \left(\sigma_i^z \sigma_{i+1}^z - 1 \right) \right] + \mathcal{B}_1 + \mathcal{B}_L,$$

$$\mathcal{B}_1 = \frac{\sin\eta}{\cos\omega_- + \cos\delta_-} \left[\frac{\mathrm{i}}{2}(\cos\omega_- - \cos\delta_-)\,\sigma_1^z \right.$$
$$\left. + \cos\theta_1 \sigma_1^x + \sin\theta_1 \sigma_1^y - \sin\omega_- \right],$$

$$\mathcal{B}_L = \frac{\sin\eta}{\cos\omega_+ + \cos\delta_+} \left[-\frac{\mathrm{i}}{2}(\cos\omega_+ - \cos\delta_+)\,\sigma_L^z \right.$$
$$\left. + \cos\theta_2\,\sigma_L^x + \sin\theta_2\,\sigma_L^y - \sin\omega_+ \right]. \tag{1.5}$$

Comparing this with the Hamiltonian (1.3) arising from the PASEP, we are led to the following identifications

$$Q = -\mathrm{e}^{\mathrm{i}\eta}, \qquad \sqrt{\frac{\alpha}{\gamma}} = -\mathrm{i}\mathrm{e}^{\mathrm{i}\omega_-}, \qquad \sqrt{\frac{\beta}{\delta}} = -\mathrm{i}\mathrm{e}^{\mathrm{i}\omega_+}$$

$$\mathrm{e}^{\mathrm{i}\theta_1} = \sqrt{\frac{\alpha}{\gamma}}\mu \mathrm{e}^{\lambda}, \qquad \mathrm{e}^{\mathrm{i}\theta_2} = \sqrt{\frac{\delta}{\beta}}\mu Q^{L-1}. \tag{1.6}$$

Furthermore, $\delta_\pm$ are determined via the equations

$$-\sqrt{\frac{\alpha\gamma}{pq}} = \frac{\sin\eta}{\cos\omega_- + \cos\delta_-}, \qquad -\sqrt{\frac{\beta\delta}{pq}} = \frac{\sin\eta}{\cos\omega_+ + \cos\delta_+}. \qquad (1.7)$$

As the spectrum of H cannot depend on the gauge parameter μ, it follows from (1.6) that the spectrum depends on θ_1 and θ_2 only via $\theta_1 - \theta_2$.

Although it has been known for a long time that H is integrable [37, 38], the off-diagonal boundary terms have so far precluded a determination of the spectrum of H by means of e.g. the algebraic Bethe ansatz [39]. However, recently a breakthrough was achieved [40–42] in the case where the parameters satisfy a certain constraint. In the above notations this constraint takes the form

$$\cos(\theta_1 - \theta_2) = \cos((2k+1)\eta + \omega_- + \omega_+). \qquad (1.8)$$

Here k is an integer in the interval $|k| \leq L/2$. In terms of the PASEP parameters the constraint reads

$$(Q^{L+2k} - e^\lambda)(\alpha\beta e^\lambda - Q^{L-2k-2}\gamma\delta) = 0. \qquad (1.9)$$

For given k and λ the constraint (1.9) can be satisfied in two distinct ways. Either one can choose Q as a root of the equation $Q^{L+2k} = e^\lambda$, or one can impose a relation on the boundary and bulk parameters such that the second factor in (1.9) vanishes. Curiously precisely under the latter conditions, the DEHP algebra [15] for the PASEP fails to produce the stationary state [20, 43].

Either choice results in a constraint on the allowed rates in the PASEP. In particular this implies that it is not possible to calculate current fluctuations for general values of the PASEP transition rates from the Bethe ansatz equations presented below.

However, in the case $\lambda = 0$ it is possible to satisfy the constraint (1.9) for arbitrary values of the PASEP parameters by choosing $k = -L/2$. As the condition (1.8) at first sight appears not to have any special significance in terms of the XXZ chain, it is rather remarkable that it can be identically satisfied for the PASEP.

1.1. Symmetries

The spectra of M and H are invariant under the particle-hole and left-right symmetries of the PASEP:

- Particle-hole symmetry

$$\alpha \leftrightarrow \gamma, \qquad \beta \leftrightarrow \delta, \qquad p \leftrightarrow q, \qquad \lambda \to -\lambda. \qquad (1.10)$$

- Left-right symmetry

$$\alpha \leftrightarrow \delta, \qquad \beta \leftrightarrow \gamma, \qquad p \leftrightarrow q, \qquad \lambda \to -\lambda. \qquad (1.11)$$

Both particle-hole and left-right symmetries leave the two factors in (1.9) invariant individually. There is a third symmetry which leaves (1.9) invariant, but interchanges the two factors

- Gallavotti-Cohen symmetry [44, 45] for the PASEP

$$e^\lambda \to \frac{\gamma\delta}{\alpha\beta} Q^{2L-2} e^{-\lambda}. \qquad (1.12)$$

The combination of (1.12) with a redefinition of the gauge parameter,

$$\mu \to \mu e^{\lambda} Q^{-L+1} \sqrt{\frac{\alpha\beta}{\gamma\delta}}, \tag{1.13}$$

corresponds to the interchange $\theta_1 \leftrightarrow \theta_2$. It is shown in the next section that if the constraint (1.8) is satisfied, the spectrum of H no longer depends on the difference $\theta_1 - \theta_2$. Hence (1.12) is not only a symmetry of the constraint equation (1.8), but also of the spectrum of H.

The Gallavotti-Cohen symmetry (1.12) implies the fluctuation theorem [46, 47] for the probability $P_L(J,t)$ to observe a current J on the first site at time t,

$$\frac{P_L(-J,t)}{P_L(J,t)} \sim \left(\frac{\alpha\beta}{\gamma\delta} Q^{-2L+2} \right)^{-Jt} \qquad (t \to \infty). \tag{1.14}$$

We emphasize the L dependence in (1.12) and (1.14), which disappears for symmetric hopping, $Q = 1$ [48]. It is further clear from (1.12) that the current vanishes $J = 0$ when the detailed balance condition

$$\frac{\alpha\beta}{\gamma\delta} Q^{-2L+2} = 1 \tag{1.15}$$

is satisfied [43]. Precisely the same Gallavotti-Cohen symmetry as in (1.12) was observed for the zero-range process (ZRP) with open boundaries [49]. This model is equivalent to the PASEP on an infinite lattice but with a fixed number of $L + 1$ particles and particle dependent hopping rates.

As a final remark, we note that it was realized in [36] that the constraint (1.8) has in fact an algebraic meaning and corresponds to the non-semisimplicity of an underlying Temperley-Lieb algebra, and implies the existence of indecomposable representations. Condition (1.8) can be interpreted as a generalized root of unity condition for this algebra, and it implies certain additional symmetries for the XXZ chain. It would be of interest to understand the impact of these symmetries on the spectrum of the PASEP with open boundaries‡.

2. Bethe ansatz for the XXZ Hamiltonian

The first Bethe ansatz results pertaining to the spectrum of H (1.5) were reported in [40, 41]. Subsequently it was noted on the basis of numerical computations in [42] and an analytical analysis for a special case in [50], that these initial results seemed incomplete. Instead of one set of Bethe ansatz equations, one generally needs two. Further developments were reported in [51, 52].

In order to simplify the following discussion we introduce the notations

$$a_{\pm} = \frac{2 \sin\eta \, \sin\omega_{\pm}}{\cos\omega_{\pm} + \cos\delta_{\pm}}. \tag{2.1}$$

When the constraint (1.8) is satisfied for some integer k, the eigenvalues of H can be divided into two groups, $E_1(k)$ and $E_2(k)$

$$E_1(k) = -a_- - a_+ - \sum_{j=1}^{L/2-1-k} \frac{2 \sin^2\eta}{\cos 2u_j - \cos\eta}, \tag{2.2}$$

---

‡ However, we have checked that for the TASEP with open boundaries the spectrum consists of singlets only, confirming [64], and hence is diagonalisable.

$$E_2(k) = -\sum_{j=1}^{L/2+k} \frac{2\sin^2\eta}{\cos 2v_j - \cos\eta}. \tag{2.3}$$

Here the complex numbers $\{u_i\}$ and $\{v_i\}$ are solutions of the coupled algebraic equations $(i = 1, \ldots, L-1)$

$$w(u_i)^{2L} = \frac{K_-(u_i - \omega_-)K_+(u_i - \omega_+)}{K_-(-u_i - \omega_-)K_+(-u_i - \omega_+)} \prod_{\substack{j=1 \\ j\neq i}}^{L/2-1-k} \frac{S(u_i, u_j)}{S(-u_i, u_j)}, \tag{2.4}$$

$$w(v_i)^{2L} = \frac{K_-(v_i)K_+(v_i)}{K_-(-v_i)K_+(-v_i)} \prod_{\substack{j=1 \\ j\neq i}}^{L/2+k} \frac{S(v_i, v_j)}{S(-v_i, v_j)}, \tag{2.5}$$

where

$$w(u) = \frac{\sin(\eta/2 + u_i)}{\sin(\eta/2 - u_i)}, \qquad S(u, v) = \cos 2v - \cos(2\eta + 2u),$$

$$K_\pm(u) = \cos\delta_\pm + \cos(\eta + \omega_\pm + 2u). \tag{2.6}$$

We will now rewrite these equations in terms of the PASEP parameters for which it is convenient to employ the notations

$$z = -\mathrm{e}^{2\,iu}, \qquad \zeta = -\mathrm{e}^{2\,iv}, \tag{2.7}$$

and

$$v_{\alpha,\gamma} = p - q - \alpha + \gamma, \tag{2.8}$$

$$\kappa_{\alpha,\gamma}^{\pm} = \frac{1}{2\alpha}\left(v_{\alpha,\gamma} \pm \sqrt{v_{\alpha,\gamma}^2 + 4\alpha\gamma}\right). \tag{2.9}$$

We then find that,
• equations (2.2) and (2.4) are rewritten as

$$\sqrt{pq}E_1(k) = \alpha + \beta + \gamma + \delta + \sum_{j=1}^{L/2-1-k} \frac{p\left(Q^2 - 1\right)^2 z_j}{(Q - z_j)(Qz_j - 1)}, \tag{2.10}$$

$$\left[\frac{z_j Q - 1}{Q - z_j}\right]^{2L} K_1(z_j) = \prod_{l\neq j}^{L/2-1-k} \frac{z_j Q^2 - z_l}{z_j - z_l Q^2} \frac{z_j z_l Q^2 - 1}{z_j z_l - Q^2}, \quad j = 1\ldots L-1. \tag{2.11}$$

Here $K_1(z) = \tilde{K}_1(z, \alpha, \gamma)\tilde{K}_1(z, \beta, \delta)$ and

$$\tilde{K}_1(z, \alpha, \gamma) = \frac{(z + Q\kappa_{\alpha,\gamma}^+)(z + Q\kappa_{\alpha,\gamma}^-)}{(Q\kappa_{\alpha,\gamma}^+ z + 1)(Q\kappa_{\alpha,\gamma}^- z + 1)}. \tag{2.12}$$

• the second set of equations, (2.3) and (2.5), becomes

$$\sqrt{pq}E_2(k) = \sum_{j=1}^{L/2+k} \frac{p\left(Q^2 - 1\right)^2 \zeta_j}{(Q - \zeta_j)(Q\zeta_j - 1)}, \tag{2.13}$$

$$\left[\frac{\zeta_j Q - 1}{Q - \zeta_j}\right]^{2L} K_2(\zeta_j) = \prod_{l \neq j}^{L/2+k} \frac{\zeta_j Q^2 - \zeta_l}{\zeta_j - \zeta_l Q^2} \frac{\zeta_j \zeta_l Q^2 - 1}{\zeta_j \zeta_l - Q^2}, \quad j = 1 \ldots L - 1,$$

(2.14)

where $K_2(\zeta) = \tilde{K}_2(\zeta, \alpha, \gamma)\tilde{K}_2(\zeta, \beta, \delta)$ and

$$\tilde{K}_2(z, \alpha, \gamma) = \frac{(\kappa_{\alpha,\gamma}^+ \zeta + Q)(\kappa_{\alpha,\gamma}^- \zeta + Q)}{(Q\zeta + \kappa_{\alpha,\gamma}^+)(Q\zeta + \kappa_{\alpha,\gamma}^-)}.$$

(2.15)

As we have mentioned before, in the case of the PASEP, and for $\lambda = 0$, the constraint (1.9) can be satisfied by either considering symmetric hopping, $Q = 1$, or by choosing $k = -L/2$.

3. Bethe ansatz equations for the "generic" PASEP

Inspection of the second set of equations (2.13) for the choice $k = -L/2$ reveals that there exists an isolated level with energy $\mathcal{E}_0 = 0$. This is readily identified with the stationary state of the PASEP. Furthermore, *all* other eigenvalues $\mathcal{E}$ of the transition matrix M follow from the first set of equations (2.10) and (2.11), and are given by

$$\mathcal{E} = -\alpha - \beta - \gamma - \delta - \sum_{j=1}^{L-1} \frac{p\left(Q^2 - 1\right)^2 z_j}{(Q - z_j)(Qz_j - 1)},$$

(3.1)

where the complex numbers z_j satisfy the Bethe ansatz equations

$$\left[\frac{z_j Q - 1}{Q - z_j}\right]^{2L} K(z_j) = \prod_{l \neq j}^{L-1} \frac{z_j Q^2 - z_l}{z_j - z_l Q^2} \frac{z_j z_l Q^2 - 1}{z_j z_l - Q^2}, \quad j = 1 \ldots L - 1.$$

(3.2)

Here $K(z) = \tilde{K}(z, \alpha, \gamma)\tilde{K}(z, \beta, \delta)$ and

$$\tilde{K}_1(z, \alpha, \gamma) = \frac{(z + Q\kappa_{\alpha,\gamma}^+)(z + Q\kappa_{\alpha,\gamma}^-)}{(Q\kappa_{\alpha,\gamma}^+ z + 1)(Q\kappa_{\alpha,\gamma}^- z + 1)}.$$

(3.3)

In order to ease notations we set from now on, without loss of generality, $p = 1$ and hence $Q = \sqrt{q}$.

4. Symmetric Exclusion Process (SEP)

The limit of symmetric diffusion is quite special and we turn to it next. We can obtain this limit either by taking $Q \to 1$ and leaving k unspecified in the equations (2.10), (2.11) and (2.13), (2.14), or by setting $k = -L/2$ and studying the limit of the equations (3.1), (3.2) for the generic PASEP. The two procedures lead to the same results and we will follow the second for the time being.

Taking the limit $Q \to 1$ in the equations (3.1), (3.2) for the general PASEP we observe that

$$\frac{zQ - 1}{Q - z} \to -1, \qquad \frac{z_j Q^2 - z_l}{z_j - Q^2 z_l} \to 1,$$

$$\frac{z_j z_l Q^2 - 1}{z_j z_l - Q^2} \to 1, \qquad \tilde{K}(z, \alpha, \gamma) \to -\frac{\alpha z + \gamma}{\gamma z + \alpha}.$$

(4.1)

We conclude that in this limit the spectral parameters z must fulfill

$$\frac{\alpha z + \gamma}{\gamma z + \alpha} \frac{\beta z + \delta}{\delta z + \beta} = 1 \; . \tag{4.2}$$

It is easy to see that the only solutions to this equation are $z = \pm 1$. Having established the leading behaviour of the roots of the Bethe ansatz equations in the limit $Q \to 1$ we now parametrize

$$z_j = \pm 1 + \mathrm{i}\lambda_j (Q^2 - 1) \; , \tag{4.3}$$

then substitute (4.3) back into the Bethe ansatz equations (3.2), (3.1) and finally take the limit $Q \to 1$. Choosing the plus sign in (4.3), we obtain with $c(x) = (x+2)/2x$

$$\left(\frac{\lambda_j - \mathrm{i}/2}{\lambda_j + \mathrm{i}/2}\right)^{2L} \left[\frac{\lambda_j + \mathrm{i}\,c(\alpha+\gamma)}{\lambda_j - \mathrm{i}\,c(\alpha+\gamma)}\right] \left[\frac{\lambda_j + \mathrm{i}\,c(\beta+\delta)}{\lambda_j - \mathrm{i}\,c(\beta+\delta)}\right]$$
$$= \prod_{l \neq j}^{L-1} \left[\frac{\lambda_j - \lambda_l - \mathrm{i}}{\lambda_j - \lambda_l + \mathrm{i}}\right] \left[\frac{\lambda_j + \lambda_l - \mathrm{i}}{\lambda_j + \lambda_l + \mathrm{i}}\right], \quad j = 1, \ldots, L-1. \tag{4.4}$$

$$\mathcal{E} = -\alpha - \beta - \gamma - \delta - \sum_{j=1}^{L-1} \frac{1}{\lambda_j^2 + 1/4}. \tag{4.5}$$

On the other hand, choosing the minus sign in (4.3) we arrive at

$$1 = \prod_{l \neq j}^{L-1} \frac{\lambda_j - \lambda_l - \mathrm{i}}{\lambda_j - \lambda_l + \mathrm{i}} \frac{\lambda_j + \lambda_l - \mathrm{i}}{\lambda_j + \lambda_l + \mathrm{i}} \; , \qquad j = 1, \ldots, L-1. \tag{4.6}$$

$$\mathcal{E} = -\alpha - \beta - \gamma - \delta \; . \tag{4.7}$$

We observe that for this choice of sign in (4.3) we obtain only a single energy level.

For both choices there is a subtlety: we have implicitly assumed that the λ_j's remain finite when we take the limit $Q \to 1$ and this need not be the case. A numerical analysis of the Bethe ansatz equations (3.2) for $Q \approx 1$ shows that we have to allow one or several λ_j's to be strictly infinite, in which case they are taken to drop out of (4.4) §. This then leads to the following set of Bethe ansatz equations, in which we only allow solutions where all spectral parameters λ_j are finite

$$\left(\frac{\lambda_j - \mathrm{i}/2}{\lambda_j + \mathrm{i}/2}\right)^{2L} \frac{\lambda_j + \mathrm{i}\,c(\alpha+\gamma)}{\lambda_j - \mathrm{i}\,c(\alpha+\gamma)} \frac{\lambda_j + \mathrm{i}\,c(\beta+\delta)}{\lambda_j - \mathrm{i}\,c(\beta+\delta)}$$
$$= \prod_{l \neq j}^{N} \frac{\lambda_j - \lambda_l - \mathrm{i}}{\lambda_j - \lambda_l + \mathrm{i}} \frac{\lambda_j + \lambda_l - \mathrm{i}}{\lambda_j + \lambda_l + \mathrm{i}} \; , j = 1, \ldots, N. \tag{4.8}$$

$$\mathcal{E} = -\alpha - \beta - \gamma - \delta - \sum_{j=1}^{N} \frac{1}{\lambda_j^2 + 1/4}. \tag{4.9}$$

Here N is allowed to take the values $1, 2, \ldots L-1$.

Curiously, the limit of symmetric exclusion can be described by a second set of Bethe ansatz equations. Taking the limit $Q \to 1$ of (2.13), (2.14) and leaving k

§ We have verified this prescription by solving the Bethe ansatz equations numerically for small systems in the vicinity of the limit $Q \to 1$.

unspecified we arrive at $\mathcal{E} = 0$ or

$$\left(\frac{\lambda_j - \mathrm{i}/2}{\lambda_j + \mathrm{i}/2}\right)^{2L} \frac{\lambda_j + \mathrm{i}\, d(\alpha + \gamma)}{\lambda_j - \mathrm{i}\, d(\alpha + \gamma)} \frac{\lambda_j + \mathrm{i}\, d(\beta + \delta)}{\lambda_j - \mathrm{i}\, d(\beta + \delta)}$$

$$= \prod_{l \neq j}^{N} \frac{\lambda_j - \lambda_l - \mathrm{i}}{\lambda_j - \lambda_l + \mathrm{i}} \frac{\lambda_j + \lambda_l - \mathrm{i}}{\lambda_j + \lambda_l + \mathrm{i}} \, , j = 1, \ldots, N, \qquad (4.10)$$

$$\mathcal{E} = -\sum_{j=1}^{N} \frac{1}{\lambda_j^2 + 1/4}. \qquad (4.11)$$

Here

$$d(x) = c(-x) = \frac{x - 2}{2x}. \qquad (4.12)$$

Apart from a constant shift in energy the two sets of equations are related by the simultaneous interchange $\alpha \leftrightarrow -\gamma$ and $\beta \leftrightarrow -\delta$. Importantly, equations (4.10) coincide with the Bethe ansatz equations derived in [53] by completely different means. Numerical studies of small systems suggest that either set (4.4) or (4.8) gives the complete spectrum of the Hamiltonian.

Interestingly, the Bethe equations (4.8) and (minus) the expression for the energy (4.9) are identical to the ones for the open Heisenberg chain with boundary magnetic fields [54, 55] ‖

$$H = -2 \sum_{j=1}^{L-1} \left[\mathbf{S}_j \cdot \mathbf{S}_{j+1} - \frac{1}{4} \right] - \frac{1}{\xi_-} \left[S_1^z + \frac{1}{2} \right] - \frac{1}{\xi_+} \left[S_L^z + \frac{1}{2} \right], \quad (4.13)$$

where $\xi_- = -1/(\alpha + \gamma)$ and $\xi_+ = -1/(\beta + \delta)$, if the reference state in the Bethe ansatz is chosen to be the ferromagnetic state with all spins up. On the other hand, the Bethe equations (4.10) and (minus) the expression for the energy (4.11) are obtained when the reference state is chosen as the ferromagnetic state with all spins down. This on the one hand shows the equivalence of the two sets of Bethe equations and on the other hand establishes the fact, that the spectrum of the SEP with open, particle number non-conserving boundary conditions (which corresponds to the z-component of total spin S^z not being a good quantum number in the spin-chain language) is identical to the spectrum of the open Heisenberg chain with boundary magnetic fields, for which S^z is a conserved quantity. This spectral equivalence is more easily established by means of a similarity transformation, see section 6.5.1 [4] and [56] for the case at hand and [57] for a general discussion on spectral equivalences for conserving and non-conserving spin chains.

The first excited state for the SEP occurs in the sector $N = 1$ of (4.10). The solution to the Bethe ansatz equations for large L is

$$\lambda_1 = \frac{L}{\pi} - \frac{1}{\pi} \left[d(\alpha + \gamma) + d(\beta + \delta) \right] - \frac{\pi}{12L}$$
$$- \frac{\pi}{6L^2} \left[d(\alpha + \gamma) - 2d^3(\alpha + \gamma) + d(\beta + \delta) - 2d^3(\beta + \delta) \right] + \ldots (4.14)$$

The corresponding eigenvalue of the transition matrix scales like L^{-2} with a coefficient that is independent of the boundary rates

$$\mathcal{E}_1(L) = -\frac{\pi^2}{L^2} + \mathcal{O}(L^{-3}). \qquad (4.15)$$

‖ We note that for symmetric diffusion the eigenvalues of the transition matrix are simply minus the corresponding eigenvalues of the Heisenberg Hamiltonian.

We conclude that for the SEP the large time relaxational behaviour is diffusive and universal.

5. Totally Asymmetric Exclusion Process (TASEP)

We now turn to the limit of totally asymmetric exclusion $Q = 0$ and set $\gamma = \delta = 0$ in order to simplify the analysis.

5.1. Stationary State Phase Diagram

The stationary state phase diagram for the TASEP was determined in [15, 16, 58] and features four distinct phases, see Figure 2:

1. A low density phase for $\alpha < 1/2$, $\alpha < \beta$.
   In the low-density phase the current in the thermodynamic limit is equal to $J = \alpha(1 - \alpha)$ and the density profile in the bulk is constant $\rho = \alpha$.
2. A high density phase for $\beta < 1/2$, $\beta < \alpha$.
   Here the current in the thermodynamic limit is equal to $J = \beta(1 - \beta)$ and the density profile in the bulk is constant $\rho = 1 - \beta$.
3. A coexistence line at $\beta = \alpha < 1/2$.
   On the coexistence line the current is equal to $J = \alpha(1 - \alpha)$, but the density profile increases linearly in the bulk $\rho(x) = \alpha + (1 - 2\alpha)x$.
4. A maximal current phase at $\alpha, \beta > 1/2$.
   This phase is characterized by the current taking the maximal possible value $J = 1/4$ and the bulk density being constant and equal to $\rho = 1/2$.

In [16] a further subdivision of the low and high density phases was proposed on the basis of differences in the behaviour of the density profile in the vicinity of the boundaries. In the high-density phase this distinction corresponds to the parameter regimes $\alpha < 1/2$ and $\alpha > 1/2$, respectively.
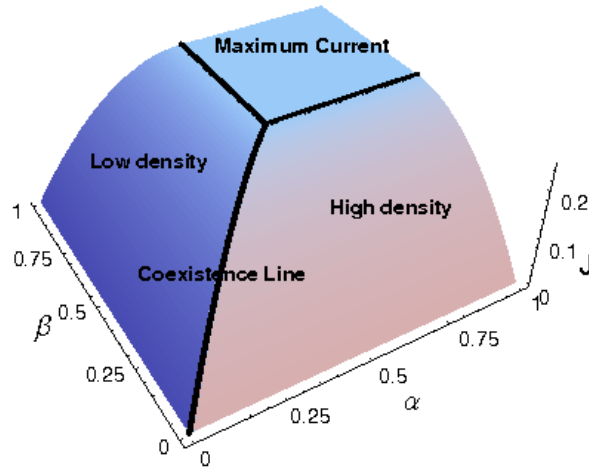
Figure 2. Stationary phase diagram determined by the current of the TASEP.

5.2. Analysis of the Bethe ansatz equations

In order to determine the exact value of the spectral gap we will now analyse (3.1) and (3.2) in the limit $L \to \infty$.

After rescaling $z \to Qz$ and setting $\gamma = \delta = 0$, the $Q \to 0$ limit of equations (3.1) and (3.2) reads

$$\mathcal{E} = -\alpha - \beta - \sum_{l=1}^{L-1} \frac{z_l}{z_l - 1}, \tag{5.1}$$

$$\left(\frac{(z_j - 1)^2}{z_j} \right)^L = (z_j + a)(z_j + b) \prod_{l \neq j}^{L-1} \left(z_j - z_l^{-1} \right). \tag{5.2}$$

In order to ease notations in what follows, we introduce

$$g(z) = \ln \left(\frac{z}{(z-1)^2} \right), \tag{5.3}$$

$$g_{\mathrm{b}}(z) = \ln \left(\frac{z}{1-z^2} \right) + \ln(z+a) + \ln(z+b), \tag{5.4}$$

where

$$a = \frac{1}{\alpha} - 1, \qquad b = \frac{1}{\beta} - 1. \tag{5.5}$$

The central object of our analysis is the "counting function" [59–61],

$$\mathrm{i}Y_L(z) = g(z) + \frac{1}{L}g_{\mathrm{b}}(z) + \frac{1}{L} \sum_{l=1}^{L-1} K(z_l, z), \tag{5.6}$$

where $K(w, z)$ is given by

$$K(w, z) = -\ln w + \ln(1 - wz). \tag{5.7}$$

Using the counting function, the Bethe ansatz equations (5.2) can be cast in logarithmic form as

$$Y_L(z_j) = \frac{2\pi}{L} I_j, \qquad j = 1, \dots, L-1. \tag{5.8}$$

Here I_j are integer numbers. The eigenvalues (5.1) of the transition matrix can be expressed in terms of the counting function as

$$\mathcal{E} = -\alpha - \beta - L \lim_{z \to 1} \left(\mathrm{i} Y_L'(z) - g'(z) - \frac{1}{L}g_{\mathrm{b}}'(z) \right). \tag{5.9}$$

Each set of integers $\{I_j | j = 1, \dots, L-1\}$ in (5.8) specifies a particular excited state. In order to determine which set corresponds to the first excited state, we have calculated the eigenvalues of the transition matrix numerically for small systems of up to $L = 14$ sites for many different values of α and β. By comparing these with the results of a numerical solution of the Bethe ansatz equations, we arrive at the conclusion that the first excited state always corresponds to the same set of integers

$$I_j = -L/2 + j \quad \text{for} \quad j = 1, \dots, L-1. \tag{5.10}$$

The corresponding roots lie on a simple curve in the complex plane, which approaches a closed contour as $L \to \infty$. The latter fact is more easily appreciated by considering the locus of reciprocal roots z_j^{-1} rather than the locus of roots z_j. In Figure 3 we

present results for $\alpha = \beta = 0.3$ and $\alpha = \beta = 0.7$ respectively. The limiting shape of the curve is that of the cardioid, which can be seen as follows. Assuming that the last term in (5.6) is approximately constant as $L \to \infty$ and using (5.8), (5.10) we find that

$$\exp(-g(z_j)) = (z_j^{1/2} - z_j^{-1/2})^2 = \chi e^{-2\pi i j/L} \qquad (L \to \infty). \qquad (5.11)$$

Here $\chi = \chi(\alpha, \beta)$ is some constant. Parametrising $z = \rho e^{i\theta}$ and multiplying (5.11) by its complex conjugate, we conclude that the roots lie on the curve defined by

$$\rho^2 - (\chi + 2\cos\theta)\rho + 1 = 0, \qquad (5.12)$$

the defining equation of the cardioid.
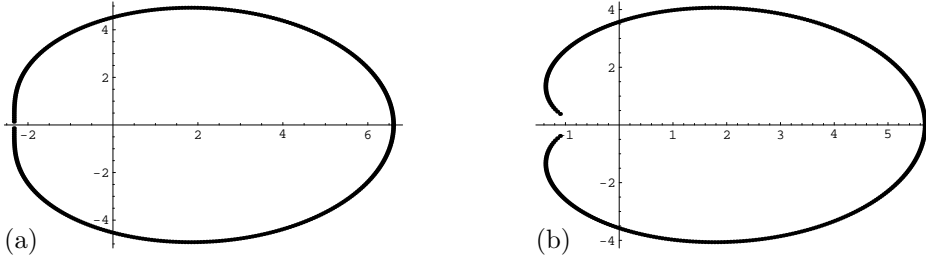
Figure 3. Reciprocal root distributions for (a) $\alpha = \beta = 0.3$ and (b) $\alpha = \beta = 0.7$, both with $L = 2n = 398$

The shape of the locus of inverse roots depends on the rates α and β. For example, in the case $\alpha = \beta = 0.7$ shown in Figure 3(b), a cusp is seen to develop at the intercept of the curve with the negative real axis (which occurs at $z = -1$ in the limit $L \to \infty$). In terms of the parameter χ characterizing the cardioid the cusp develops at $\chi = 4$. In contrast, no cusp occurs for $\alpha = \beta = 0.3$ as shown in Figure 3(a).¶ We will see that this difference in the shape of the loci of inverse roots is reflected in a profoundly different finite-size scaling behaviour of the corresponding spectral gaps.

In order to compute the exact large L asymptotics of the spectral gap, we derive an integro-differential equation for the counting function $Y_L(z)$ in the limit $L \to \infty$. As a simple consequence of the residue theorem we can write

$$\frac{1}{L}\sum_{j=1}^{L-1} f(z_j) = \oint_{C_1+C_2} \frac{dz}{4\pi i} \, f(z)Y_L'(z)\cot\left(\frac{1}{2}LY_L(z)\right), \qquad (5.13)$$

where $C = C_1 + C_2$ is a contour enclosing all the roots z_j, C_1 being the "interior" and C_2 the "exterior" part, see Figure 4. The contours C_1 and C_2 intersect in appropriately chosen points ξ and ξ^*. It is convenient to fix the end points ξ and ξ^* by the requirement
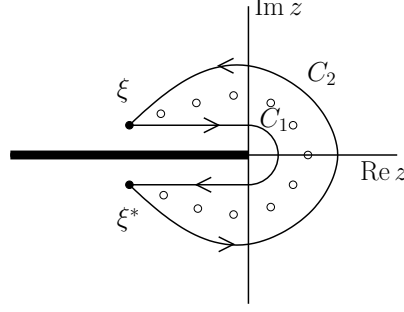
$$Y_L(\xi^*) = -\pi + \frac{\pi}{L}, \qquad Y_L(\xi) = \pi - \frac{\pi}{L}. \qquad (5.14)$$

Using the fact that integration from ξ^* to ξ over the contour formed by the roots is equal to half that over $C_2 - C_1$ we find,

$$i Y_L(z) = g(z) + \frac{1}{L}g_b(z) + \frac{1}{2\pi}\int_{\xi^*}^{\xi} K(w,z)Y_L'(w)dw$$

$$+ \frac{1}{2\pi}\int_{C_1} \frac{K(w,z)Y_L'(w)}{1 - e^{-iLY_L(w)}}\,dw + \frac{1}{2\pi}\int_{C_2} \frac{K(w,z)Y_L'(w)}{e^{iLY_L(w)} - 1}\,dw, \qquad (5.15)$$

¶ This corresponds to having $\chi > 4$.

where we have chosen the branch cut of $K(w, z)$ to lie along the negative real axis.

Figure 4. Sketch of the contour of integration C in (5.13). The open dots correspond to the roots z_j and ξ is chosen close to z_{L-1} and avoiding poles of $\cot(LY_L(z)/2)$.

Our strategy is to solve the integro-differential equation (5.15) by iteration and then use the result to obtain the eigenvalue of the transition matrix from equation (5.9).

6. Low and High Density Phases

In the low and high density phases the locations of the end points ξ and ξ^* are such that a straightforward expansion of (5.15) in inverse powers of L is possible (see e.g. [62,63] and Appendix A). The result is

$$
\mathrm{i}\, Y_L(z) = g(z) + \frac{1}{L} g_{\mathrm{b}}(z) + \frac{1}{2\pi} \int_{\xi^*}^{\xi} K(w, z) Y_L'(w) \mathrm{d}w
$$
$$
+ \frac{\pi}{12 L^2} \left(\frac{K'(\xi^*, z)}{Y_L'(\xi^*)} - \frac{K'(\xi, z)}{Y_L'(\xi)} \right) + \mathcal{O}(L^{-4})
$$
$$
= g(z) + \frac{1}{L} g_{\mathrm{b}}(z) + \frac{1}{2\pi} \int_{z_{\mathrm{c}}^-}^{z_{\mathrm{c}}^+} K(w, z) Y_L'(w) \mathrm{d}w
$$
$$
+ \frac{1}{2\pi} \int_{\xi^*}^{z_{\mathrm{c}}^-} K(w, z) Y_L'(w) \mathrm{d}w + \frac{1}{2\pi} \int_{z_{\mathrm{c}}^-}^{\xi} K(w, z) Y_L'(w) \mathrm{d}w
$$
$$
+ \frac{\pi}{12 L^2} \left(\frac{K'(\xi^*, z)}{Y_L'(\xi^*)} - \frac{K'(\xi, z)}{Y_L'(\xi)} \right) + \mathcal{O}(L^{-4}) , \tag{6.1}
$$

where the derivatives of K are with respect to the first argument. We note that here we have implicitly assumed that $Y_L'(\xi)$ is nonzero and of order $\mathcal{O}(L^0)$. In order to find the eigenvalue of the transition matrix (5.9) up to second order in inverse powers of L, we will need to solve (6.1) perturbatively to third order. Substituting the expansions

$$
Y_L(z) = \sum_{n=0}^{\infty} L^{-n} y_n(z), \qquad \xi = z_{\mathrm{c}} + \sum_{n=1}^{\infty} L^{-n}(\delta_n + \mathrm{i}\eta_n), \tag{6.2}
$$

back into (6.1) yields a hierarchy of equations for the functions $y_n(z)$ of the type

$$
y_n(z) = g_n(z) + \frac{1}{2\pi \mathrm{i}} \int_{z_{\mathrm{c}}^-}^{z_{\mathrm{c}}^+} K(w, z) y_n'(w) \, \mathrm{d}w, \tag{6.3}
$$

where $z_{\mathrm{c}}^{\pm} = z_{\mathrm{c}} \pm \mathrm{i}0$. The integral is along the closed contour following the locus of the roots. The first few driving terms $g_n(z)$ are given by

$$
\begin{aligned}
g_0(z) &= -\mathrm{i}g(z), \\
g_1(z) &= -\mathrm{i}g_{\mathrm{b}}(z) + \kappa_1 + \lambda_1 \tilde{K}(z_{\mathrm{c}}, z), \\
g_2(z) &= \kappa_2 + \lambda_2 \tilde{K}(z_{\mathrm{c}}, z) + \mu_2 K'(z_{\mathrm{c}}, z), \\
g_3(z) &= \kappa_3 + \lambda_3 \tilde{K}(z_{\mathrm{c}}, z) + \mu_3 K'(z_{\mathrm{c}}, z) + \nu_3 K''(z_{\mathrm{c}}, z).
\end{aligned}
\tag{6.4}
$$

We recall that the functions g and g_{b} are defined in (5.3) and (5.4) and $\tilde{K}(z_{\mathrm{c}}, z) = \ln(z - z_{\mathrm{c}}^{-1})$. The coefficients κ_n, λ_n, μ_n and ν_n are given in terms of δ_n, η_n defined by (6.2) as well as derivatives of y_n evaluated at z_{c}. Explicit expressions are presented in Appendix B.

These coefficients as well as z_{c} are determined self-consistently by solving (6.3) and then imposing the boundary conditions (5.14).

6.1. Small values of α and β

When α and β are small we assume that the singularities in $g_{\mathrm{b}}(z)$, i.e. the points $-a = 1 - 1/\alpha$ and $-b = 1 - 1/\beta$, lie outside the contour of integration. From the distribution of the reciprocal roots, Figure 3(a), we further infer that for small values of α and β the roots lie inside the unit circle. In particular we assume that $z_{\mathrm{c}} \neq -1$ and that the points ± 1 lie outside the contour of integration.

We now proceed to solve (6.3) and then verify a posteriori that the above assumptions hold.

The equation (6.3) for $n = 0$ is solved by the simple ansatz

$$
y_0(z) = \kappa_0 + g_0(z) .
\tag{6.5}
$$

Substituting the ansatz into the integro-differential equation (6.3) for $n = 0$ we find that

$$
\begin{aligned}
\kappa_0 &= -\frac{1}{2\pi} \int_{z_{\mathrm{c}}^-}^{z_{\mathrm{c}}^+} (-\ln w + \ln(1 - wz)) \left(\frac{1}{w} - \frac{2}{w-1} \right) \mathrm{d}w \\
&= -\mathrm{i}\left(-\ln(-z_{\mathrm{c}}) + 2\ln(1 - z_{\mathrm{c}}) \right).
\end{aligned}
\tag{6.6}
$$

This in turn implies that the zeroth order term in the expansion of the counting function is given by

$$
y_0(z) = -\mathrm{i}\ln \left[-\frac{z}{z_{\mathrm{c}}} \left(\frac{1 - z_{\mathrm{c}}}{1 - z} \right)^2 \right].
\tag{6.7}
$$

In order to derive this result we have made use of the following simple but useful identity (C denotes the contour of integration from z_{c}^- to z_{c}^+)

$$
\frac{1}{2\pi\mathrm{i}} \int_{z_{\mathrm{c}}^-}^{z_{\mathrm{c}}^+} \frac{\ln w}{w + x} \, \mathrm{d}w = \begin{cases} \ln(1 + z_{\mathrm{c}}/x) & \text{if } -x \text{ outside } C, \\ \ln(-x - z_{\mathrm{c}}) & \text{if } -x \text{ inside } C. \end{cases}
\tag{6.8}
$$

The integro-differential equations for $n = 1, 2, 3$ are solved in an analogous manner, with the results

$$
\begin{aligned}
y_1(z) = & -\mathrm{i}\ln \left[-\frac{z}{z_{\mathrm{c}}} \frac{1 - z_{\mathrm{c}}^2}{1 - z^2} \left(\frac{z_{\mathrm{c}} - z_{\mathrm{c}}^{-1}}{z - z_{\mathrm{c}}^{-1}} \right)^{-\mathrm{i}\lambda_1} \frac{z + a}{z_{\mathrm{c}} + a} \frac{z + b}{z_{\mathrm{c}} + b} \right] \\
& + \kappa_1 - \mathrm{i}\ln \left(ab(-z_{\mathrm{c}})^{-\mathrm{i}\lambda_1} \right),
\end{aligned}
\tag{6.9}
$$

$$y_2(z) = \lambda_2 \ln\left(\frac{z_c - z_c^{-1}}{z - z_c^{-1}}\right) + \frac{\mu_2}{z_c^2}\left(\frac{1}{z - z_c^{-1}} - \frac{1}{z_c - z_c^{-1}}\right)$$

$$+ \kappa_2 - \lambda_2 \ln(-z_c) - \frac{\mu_2}{z_c}, \tag{6.10}$$

$$y_3(z) = \lambda_3 \ln\left(\frac{z_c - z_c^{-1}}{z - z_c^{-1}}\right) + \left(\frac{\mu_3}{z_c^2} - \frac{\nu_3}{z_c^3}\right)\left(\frac{1}{z - z_c^{-1}} - \frac{1}{z_c - z_c^{-1}}\right)$$

$$- \frac{\nu_3}{z_c^3}\left(\frac{z}{(z - z_c^{-1})^2} - \frac{z_c}{(z_c - z_c^{-1})^2}\right) + \kappa_3 - \lambda_3 \ln(-z_c)$$

$$- \left(\frac{\mu_3}{z_c} - \frac{\nu_3}{z_c^2}\right). \tag{6.11}$$

The coefficients κ_n, λ_n, μ_n and ν_n are given in terms of δ_n, η_n and derivatives of y_n at z_c, see Appendix B and we now proceed to determine them. Substituting the expansions (6.2) into equation (5.14), which fixes the endpoints ξ and ξ^*, we obtain a hierarchy of conditions for $y_n(z_c)$, e.g.

$$Y_L(\xi) = y_0(\xi) + \frac{1}{L}y_1(\xi) + \frac{1}{L^2}y_2(\xi) + \dots$$

$$= y_0(z_c) + \frac{1}{L}\left[y_1(z_c) + y_0'(z_c)(\delta_1 + i\eta_1)\right] + \dots$$

$$= \pi - \frac{\pi}{L}. \tag{6.12}$$

Solving these order by order we obtain

$$\lambda_1 = 2i,$$

$$\lambda_3 = \mu_2 = \lambda_2 = \kappa_1 = 0, \tag{6.13}$$

$$\nu_3 = z_c\mu_3 = z_c(z_c - 1)^2\kappa_2 = -i\pi^2 z_c^2\left(\frac{z_c - 1}{z_c + 1}\right)^2,$$

with κ_3 undetermined. Furthermore, the intersect of the solution curve with the negative real axis in the limit $L \to \infty$ is found to be

$$z_c = -\frac{1}{\sqrt{ab}}. \tag{6.14}$$

Having determined the counting function, we are now in a position to evaluate the corresponding eigenvalue of the transition matrix from equation (5.9)

$$\mathcal{E}_1(L) = -\alpha - \beta - \frac{2z_c}{1 - z_c} - \frac{\pi^2}{z_c - z_c^{-1}}\frac{1}{L^2} + \mathcal{O}\left(L^{-3}\right)$$

$$= -\alpha - \beta + \frac{2}{1 + \sqrt{ab}} - \frac{\pi^2}{\sqrt{ab} - 1/\sqrt{ab}}\frac{1}{L^2} + \mathcal{O}\left(L^{-3}\right). \tag{6.15}$$

We conclude that to leading order in L, the eigenvalue of the transition matrix with the second largest real part is a nonzero constant. This implies an exponentially fast relaxation to the stationary state at large times. We note that due to the symmetry of the root distribution corresponding to (5.10) under complex conjugation $\mathcal{E}_1$ is in fact real. The domain of validity of (6.15) is determined by the initial assumption that $-a$ and $-b$ lie outside the contour of integration, i.e.

$$-a < z_c \quad \text{and} \quad -b < z_c. \tag{6.16}$$

The parameter regime in α and β in which (6.15) is valid is therefore bounded by the curves

$$
\begin{aligned}
\beta_{\mathrm{c}} &= \left[1 + \left(\frac{\alpha}{1-\alpha}\right)^{1/3}\right]^{-1}, \quad 0 \leq \alpha < \frac{1}{2}, \\
\alpha_{\mathrm{c}} &= \left[1 + \left(\frac{\beta}{1-\beta}\right)^{1/3}\right]^{-1}, \quad 0 \leq \beta < \frac{1}{2}.
\end{aligned}
\tag{6.17}
$$

6.1.1. Coexistence Line   On the line $\beta = \alpha$, the leading term in (6.15) vanishes and the eigenvalue with the largest real part different from zero is therefore

$$
\mathcal{E}_1(L) = -\frac{\pi^2 \alpha(1-\alpha)}{1-2\alpha}\frac{1}{L^2} + \mathcal{O}(L^{-3}).
\tag{6.18}
$$

This equation holds for fixed $\alpha < 1/2$ and $L \to \infty$. We note that there is a divergence for $\alpha \to 1/2$, signaling the presence of a phase transition. The inverse proportionality of the eigenvalue (6.18) to the square of the system size implies a dynamic exponent $z = 2$, which suggests that the dominant relaxation at large times is governed by diffusive behaviour. As shown in [29, 30] the diffusive nature of the relaxational mechanism can in fact be understood in terms of the unbiased random walk behaviour of a shock (domain wall between a low and high density region). Our results (6.15) and (6.18) for the phase domain given by (6.17) and the coexistence line agree with the relaxation time calculated in the framework of a domain wall theory (DWT) model in [30]. As we will show next, this is in contrast to the massive phases beyond the phase boundaries (6.17), where the exact result will differ from the DWT prediction. In Section 9 we present a modified DWT framework that allows us to understand the phase boundaries (6.17).

6.2. Massive phase II:

In this section we will treat the case $-b > z_{\mathrm{c}}$ with $-a < z_{\mathrm{c}}$ as before. The case $-a > z_{\mathrm{c}}$ with $-b < z_{\mathrm{c}}$ is obtained by the interchange $\alpha \leftrightarrow \beta$ in the relevant formulas.

We need to solve the same integral equation (6.3) as before; in particular the driving terms g_n defined in (6.4) remain unchanged. However, when iterating the driving term $g_1(z)$ there is an extra contribution because the pole at $-b$ now lies inside the integration contour, see (6.8). As a result the solution for $y_1(z)$ is now of the form

$$
\begin{aligned}
y_1(z) = {}& -\mathrm{i}\ln\left[-\frac{z}{z_{\mathrm{c}}}\frac{1-z_{\mathrm{c}}^2}{1-z^2}\left[\frac{z_{\mathrm{c}}-z_{\mathrm{c}}^{-1}}{z-z_{\mathrm{c}}^{-1}}\right]^{-\mathrm{i}\lambda_1}\frac{z+a}{z_{\mathrm{c}}+a}\frac{z+b}{z_{\mathrm{c}}+b}\frac{z+1/b}{z_{\mathrm{c}}+1/b}\right] \\
& + \kappa_1 - \mathrm{i}\ln\left(a(-z_{\mathrm{c}})^{-\mathrm{i}\lambda_1}\right).
\end{aligned}
\tag{6.19}
$$

The forms of the solutions for y_n for $n \geq 2$ remain unchanged. The coefficients of the various terms are again fixed by imposing the boundary condition (5.14), with the result

$$
\begin{aligned}
&\lambda_1 = 3\mathrm{i}, \\
&\lambda_3 = \mu_2 = \lambda_2 = \kappa_1 = 0, \\
&\nu_3 = z_{\mathrm{c}}\mu_3 = \frac{3}{2}z_{\mathrm{c}}(z_{\mathrm{c}}-1)^2\kappa_2 = -4\mathrm{i}\pi^2 z_{\mathrm{c}}^2\left(\frac{z_{\mathrm{c}}-1}{z_{\mathrm{c}}+1}\right)^2,
\end{aligned}
\tag{6.20}
$$

and κ_3 again remains undetermined. We note that the difference in the functional form of $y_1(z)$ compared to (6.9) affects the coefficients in all subleading contributions $y_2(z)$, $y_3(z)$ etc. The intersect of the locus of roots with the negative real axis in the limit $L \to \infty$ is now given by

$$z_{\rm c} = -\frac{1}{\sqrt{ab_{\rm c}}} = -a^{-1/3} = -\left[\frac{\alpha}{1-\alpha}\right]^{1/3}, \tag{6.21}$$

where we have defined

$$b_{\rm c} = \frac{1-\beta_{\rm c}}{\beta_{\rm c}}. \tag{6.22}$$

The eigenvalue of the transition matrix with the largest nonzero real part is again determined from (5.9)

$$\mathcal{E}_1(L) = -\alpha - \frac{1+2z_{\rm c}}{1-z_{\rm c}} - \frac{4\pi^2}{z_{\rm c} - z_{\rm c}^{-1}}\frac{1}{L^2} + \mathcal{O}\left(L^{-3}\right)$$

$$= -\alpha - \beta_{\rm c} + \frac{2}{1+a^{1/3}} - \frac{4\pi^2}{a^{1/3} - a^{-1/3}}\frac{1}{L^2} + \mathcal{O}\left(L^{-3}\right). \tag{6.23}$$

The result (6.23) is valid in the regime

$$0 \le \alpha < 1/2, \qquad \beta_{\rm c} \le \beta \le 1, \tag{6.24}$$

and is seen to be independent of β. Hence in this phase the relaxation to the stationary state at large times is independent of the extraction rate at the right-hand boundary of the system.

7. Maximum Current Phase

In the maximum current phase $\alpha, \beta > 1/2$ the above analysis of the integro-differential equation (5.15) breaks down. The primary reason for this is that the locus of roots now closes at $z_{\rm c} = -1$ for $L \to \infty$ and this precludes a Taylor expansion of the kernel $K(w,z)$ around $w = \xi$. A more detailed discussion of the complications arising from $z_{\rm c} = -1$ is presented in Appendix A.

In order to determine the large-L behaviour of the eigenvalues of the transition matrix with the largest real parts in the maximum current phase, we have resorted to a direct numerical solution of the Bethe ansatz equations (3.2) for lattices of up to $L = 2600$ sites. In order to facilitate a finite-size scaling analysis it is necessary to work with quadruple precision (32 digits in C) at large L. We find that the leading behaviour of the spectral gap in the limit $L \to \infty$ in the maximum current phase is independent of the boundary rates α and β.

7.1. Leading behaviour

In Figure 5 we plot the numerical results for eigenvalue $\mathcal{E}_1$ of the first excited state for $\alpha = \beta = 0.7$ as a function of the inverse system size L^{-1} on a double-logarithmic scale. The almost straight line suggests an algebraic behaviour at large L

$$\mathcal{E}_1(L) \sim -eL^{-s} \qquad (L \to \infty). \tag{7.1}$$

A simple least-square fit of the graph in Figure 5 in the region $2200 \le L \le 2600$ to a straight line gives a slope of $s \approx 1.493$, which is close to the expected value $3/2$.
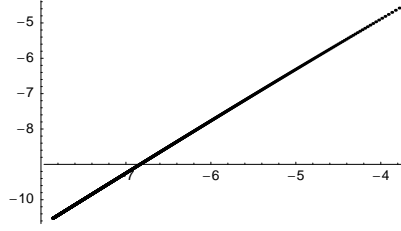
Figure 5. Double logarithmic plot of $-\mathcal{E}_1(L)$ as a function of $1/L$ for $\alpha = \beta = 0.7$

A better result is obtained by extrapolating our finite-size data as follows. We first divide the data set for $\mathcal{E}_1(L)$ into bins containing 11 data points each. The kth bin B_k is defined by taking $20k \leq L \leq 20(k+1)$. Within each bin we fit the data for $\mathcal{E}_1(L)$ to a functional form

$$\mathcal{E}_1(L) \approx -e_k L^{-s_k}. \tag{7.2}$$

We have implemented this procedure for $100 \leq k \leq 128$ and obtained a sequence of exponents s_k. We observe that the following least-square fit of the sequence s_k to a polynomial gives excellent agreement

$$s_k \approx 1.4999949 - 0.7822533k^{-1} + 3.8014387k^{-2}. \tag{7.3}$$

Finally, we extrapolate to $k = \infty$ and obtain

$$s_\infty \approx 1.4999949. \tag{7.4}$$

This is very close to the expected result $s = 3/2$. The polynomial fit as well as the extrapolation is shown in Figure 6.
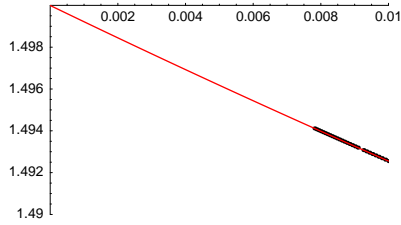
Figure 6. Polynomial fit to the exponents s_k of (7.2) plotted against $1/k$ for $\alpha = \beta = 0.7$. Extrapolation gives an exponent $s_\infty = 1.5$.

7.2. Subleading corrections

Having established that the leading behaviour of $\mathcal{E}_1(L)$ at large L is as $L^{-3/2}$, we now turn to subleading corrections. Assuming that

$$\mathcal{E}_1(L) \sim -eL^{-3/2} - fL^{-d} , \qquad (L \to \infty), \tag{7.5}$$

we wish to determine the value of the exponent d. To this end, we define the sequence

$$\Delta_L = \frac{L}{2} \left[(L+2)^{3/2}\mathcal{E}_1(L+2) - L^{3/2}\mathcal{E}_1(L) \right]. \tag{7.6}$$

If (7.5) is correct, we expect Δ_L to be proportional to $L^{3/2-d}$ at large L. In Figure 7 we plot Δ_L as a function of L^{-1} in a double-logarithmic plot. The result is well approximated by a straight line with slope 0.95, which suggests that the exponent of the subleading corrections is $d = 5/2$.
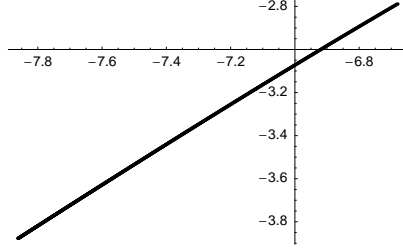
Figure 7. Double logarithmic plot of Δ_L as a function of $1/L$ for $\alpha = \beta = 0.7$ and $800 \leq L \leq 2600$.

A more accurate estimate of the exponent can be obtained by extrapolating the finite-size data along the same lines as before. We group the data for s_L into bins of 11 points each and carry out a least-square fit for each bin to a functional form

$$\Delta_L \approx e_k L^{-s_k}. \tag{7.7}$$

The resulting sequence of exponents s_k is described very well by the polynomial least-square fit

$$s_k \approx 0.998755255 - 4.329298118 k^{-1} + 8.363104997 k^{-2}. \tag{7.8}$$

Extrapolation gives $s_\infty \approx 0.998755255$, which is very close to 1. This suggests that the subleading corrections to $\mathcal{E}_1$ indeed scale like $L^{-5/2}$. The polynomial fit to the sequence of exponents s_k and the extrapolation to $k = \infty$ are shown in Figure 8.
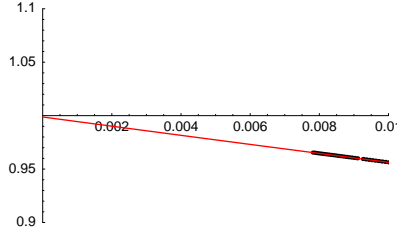
Figure 8. Polynomial fit to the exponents s_k in (7.7) plotted against $1/k$ for $\alpha = \beta = 0.7$.

7.3. Coefficient of the $L^{-3/2}$ term

Having established that asymptotically the L-dependence of the eigenvalue is given by

$$\mathcal{E}_1(L) \sim -e L^{-3/2} - f L^{-5/2} \qquad (L \to \infty), \tag{7.9}$$

we now determine the coefficient e. We again arrange the data for $\mathcal{E}_1(L)$ into bins $20k \leq L \leq 20(k+1)$ and within each bin perform least-square fits of $\mathcal{E}_1(L)$ to the functional form

$$\mathcal{E}_1(L) \approx -e_k L^{-3/2} - f_k L^{-5/2} , \quad 20k \leq L \leq 20(k+1). \tag{7.10}$$

As is shown in Figure 9, the resulting sequence of coefficients e_k for the largest available values of k ($100 \leq k \leq 128$) can be fitted very well to the polynomial

$$e_k \approx 3.5780576 - 7.2704902 k^{-2}. \tag{7.11}$$
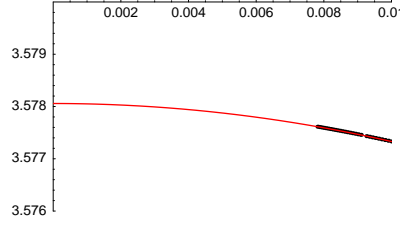
Figure 9. Polynomial fit to the coefficients e_k defined in (7.10) plotted against $1/k$ for $\alpha = \beta = 0.7$.

Extrapolation to $k \to \infty$ then gives the following result for the eigenvalue of the first excited state of the TASEP in the MC phase

$$\mathcal{E}_1(L) \approx -3.578\, L^{-3/2} + \mathcal{O}(L^{-5/2}). \tag{7.12}$$

As we have already mentioned, the behaviour (7.12) is in fact independent of α and β throughout the maximum current phase and the coefficient is a universal number.

The numerical value for the gap is smaller than that of the half-filled TASEP on a ring, where it is found that $\mathcal{E}_{1,\mathrm{ring}}(L) \sim -6.509 \ldots L^{-3/2}$ [24, 25, 64].

7.3.1. Extrapolation Procedure In order to assess the accuracy of the numerical extrapolation procedure we have employed above, it is instructive to consider the analogous analysis on the coexistence line. Here the exact analytical value for the spectral gap is known. For $\alpha = \beta = 0.3$ equation (6.18) gives

$$\mathcal{E}_1(L) = -5.1815423 \ldots L^{-2} + \mathcal{O}(L^{-3}). \tag{7.13}$$

We have computed $\mathcal{E}_1(L)$ on the coexistence line by a direct numerical solution of the Bethe ansatz equations for lattices of up to $L = 1800$ sites. Fitting $\mathcal{E}_1(L)$ to the form

$$\mathcal{E}_1(L) \approx -e_k L^{-s_k} , \quad 20k \leq L \leq 20(k+1), \tag{7.14}$$

and using the same analysis as above, but for the somewhat smaller values $61 \leq k \leq 88$, we find that the sequence of exponents s_k is well approximated by the polynomial

$$s_k \approx 2.0000967 - 0.3772271 k^{-1} + 0.7953103 k^{-2}. \tag{7.15}$$

Extrapolation to $k = \infty$ gives excellent agreement with the exact result $s = 2$. Similarly, a least-square fit of the sequence of coefficients e_k to a polynomial in $1/k$ gives

$$e_k \approx 5.1814722 - 0.0002060 k^{-1} + 0.0000782 k^{-2}. \tag{7.16}$$

The extrapolated value e_∞ agrees with the exact result (7.13) to five significant digits. This is quite satisfactory.

8. Other Gaps and Complex Eigenvalues

Having established the large-L behaviour of the eigenvalue of M corresponding to the lowest excited state, we now turn to higher excited states. As M is not Hermitian, its eigenvalues are in general complex. A complex eigenvalue in turn leads to interesting oscillatory behaviour in the time evolution. Aspects of such behaviour have been discussed for the KPZ equation [67,68]

8.1. Massive Phase I: $\alpha < \alpha_c$, $\beta < \beta_c$, $\alpha \neq \beta$

Here the next lowest excitation is obtained by choosing the integers I_j in the Bethe ansatz equations (5.6) as

$$I_j = -L/2 + j \quad \text{for} \quad j = 1, \ldots, L-2 \qquad I_{L-1} = L/2. \qquad (8.1)$$

This choice of integers I_j corresponds to a "hole" between the last two roots. Hence we will refer to this state as a "hole state". As this choice is asymmetric with respect to the interchange $j \leftrightarrow L-j$, we expect the corresponding eigenvalue to be complex. This is indeed the case for small system sizes L. However, as the system size increases, the eigenvalue becomes real at a certain *finite* value of L. This comes about in the following way. For small L, the last root has a finite imaginary part and the distribution of the other roots is asymmetric with respect to the real axis, see Figure 10(a). As L increases the last root approaches the negative real axis until above a critical value of L its imaginary part vanishes. The other roots are then arranged in complex conjugate pairs, so that the corresponding eigenvalue becomes real. An example of this is shown in Figure 10(b). Further details regarding this phenomenon are given in Appendix C.

(a) (b)
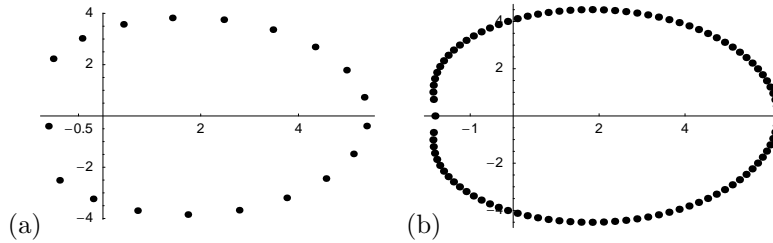
Figure 10. Reciprocal root distributions corresponding to the hole state for $\alpha = 0.3$ and $\beta = 0.4$; (a) $L = 2n = 20$ (b) $L = 2n = 100$.

Assuming that the root distribution remains as in Figure 10(b) in the limit $L \to \infty$, we can compute the corresponding eigenvalue in the following way. As z_{L-1} is an isolated root, we first write the counting function in (5.6) as

$$\mathrm{i}Y_L(z) = g(z) + \frac{1}{L}(g_\mathrm{b}(z) + K(z_{L-1}, z)) + \frac{1}{L}\sum_{l=1}^{L-2} K(z_l, z). \qquad (8.2)$$

We can now follow the same procedure as in Section 5.2 and turn this into an integro-differential equation of the form (5.15). Importantly, the endpoints of the integration contour are again complex conjugates of one another. Compared to the equation for the lowest excitation the driving term has an extra contribution of order $\mathcal{O}(L^{-1})$ and

the boundary conditions that determine the endpoints ξ and ξ^* of the contour now read

$$Y_L(\xi^*) = -\pi + \frac{\pi}{L}, \qquad Y_L(\xi) = \pi - \frac{3\pi}{L}. \tag{8.3}$$

The root $\zeta = z_{L-1}$ is determined by the requirement that

$$Y_L(\zeta) = \pi. \tag{8.4}$$

If we expand ξ, ξ^* and Y_L, but not ζ, in powers of L^{-1}, we can use the results of Section 6. With

$$Y_L(z) = \sum_{n=0}^{\infty} L^{-n} y_n(z), \tag{8.5}$$

we find the same solutions for y_0, y_2 and y_3 as in (6.7), (6.10) and (6.11). However, due to the additional term proportional to L^{-1} in (8.2), the solution for y_1 differs from that in (6.9) and is given by

$$y_1(z) = -i \ln \left[-\frac{z}{z_\mathrm{c}} \frac{1-z_\mathrm{c}^2}{1-z^2} \left(\frac{z_\mathrm{c} - z_\mathrm{c}^{-1}}{z - z_\mathrm{c}^{-1}} \right)^{-i\lambda_1} \frac{z+a}{z_\mathrm{c}+a} \frac{z+b}{z_\mathrm{c}+b} \right]$$

$$- i \ln \left[-\frac{z-1/\zeta}{z_\mathrm{c}-1/\zeta} \right] + \kappa_1 - i \ln \left(-\zeta^{-1} ab(-z_\mathrm{c})^{-i\lambda_1} \right). \tag{8.6}$$

Only now will we expand ζ,

$$\zeta = \zeta_0 + \sum_{n=1}^{\infty} L^{-n} \tilde{\delta}_n, \tag{8.7}$$

and use the definitions of the points ξ, ξ^* and ζ above. Employing again the expansion (6.2) and Appendix B, we find that the intersect of the solution curve with the negative real axis in the limit $L \to \infty$ is given, as before, by

$$z_\mathrm{c} = -\frac{1}{\sqrt{ab}}. \tag{8.8}$$

Furthermore, in leading order, the isolated root ζ tends to z_c in the limit, i.e. $\zeta_0 = z_\mathrm{c}$. Putting everything together we finally find that the eigenvalue for this solution is given by

$$\mathcal{E}_2(L) = -\alpha - \beta - \frac{2z_\mathrm{c}}{1-z_\mathrm{c}} - \frac{4\pi^2}{z_\mathrm{c} - z_\mathrm{c}^{-1}} \frac{1}{L^2} + \mathcal{O}(L^{-3}), \tag{8.9}$$

with z_c given in (8.8). It is instructive to compare $\mathcal{E}_2(L)$ to the gap of the first excited state $\mathcal{E}_1(L)$. The latter exhibits a non-analytic change at $\beta = \beta_\mathrm{c}$. Interestingly, we find that to order $\mathcal{O}(L^{-2})$

$$\lim_{\beta \uparrow \beta_\mathrm{c}} \mathcal{E}_2(L) = \lim_{\beta \downarrow \beta_\mathrm{c}} \mathcal{E}_1(L) \neq \lim_{\beta \uparrow \beta_\mathrm{c}} \mathcal{E}_1(L) . \tag{8.10}$$

In conclusion we find that in the massive phase M_I also the second gap is real and given by (8.9). The second gap may be a complex conjugate pair for small values of the system size. However, this pair merges at a *finite* value of L producing two real eigenvalues, the lowest of which is given by (8.9). This observation is consistent with the results of Dudzinski and Schütz [30], who computed the spectrum on the coexistence line $\alpha = \beta$ for small system sizes.

8.2. Coexistence line

As we have seen above, the second gap of the TASEP is real for large L, even though it may be complex for small system sizes. On the coexistence line, the leading term of (8.9) vanishes and we are left with a second diffusive mode with an eigenvalue that vanishes as $\mathcal{O}(L^{-2})$. A priori we expect a whole band of diffusive modes on the coexistence line, some of which should be given by the domain wall theory of [30],

$$\mathcal{E}_n(L) = -\frac{n^2\pi^2}{z_c - z_c^{-1}}\frac{1}{L^2} + \mathcal{O}(L^{-3}), \tag{8.11}$$

with z_c given by (8.8). It is clearly of interest to know whether or not there are complex modes as well, which would result in oscillatory behaviour in the relaxational dynamics at large times.

We observed numerically, that the first complex excitation that does not become real for a finite value of L in the massive phase M_I corresponds to the choice of integers

$$
\begin{aligned}
I_j &= -L/2 + j \quad \text{for} \quad j = 1, \ldots, L-3 \\
I_{L-2} &= L/2 - 1, \quad I_{L-1} = L/2,
\end{aligned}
\tag{8.12}
$$

i.e. there is one hole between the second and third last roots. The corresponding (reciprocal) root distribution again has an isolated root on the negative real axis, see Figure 11, which now lies inside the contour of integration.
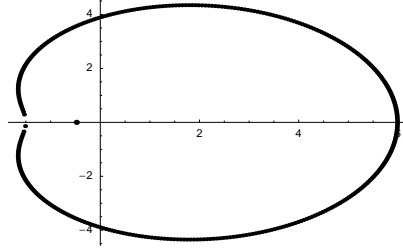
Figure 11. Reciprocal root distributions corresponding to the first complex eigenvalue $\mathcal{E}_c(L)$ for $\alpha = \beta = 0.3$ and $L = 1860$.

Proceeding as in the preceding section, we write the counting function as

$$\mathrm{i}Y_L(z) = g(z) + \frac{1}{L}(g_b(z) + K(z_{L-1}, z) + \frac{1}{L}\sum_{l=1}^{L-2} K(z_l, z). \tag{8.13}$$

Turning the sum into an integral we arrive at the following integro-differential equation

$$
\begin{aligned}
\mathrm{i}\,Y_L(z) = {}& g(z) + \frac{1}{L}\left(g_b(z) + K(\zeta_1, z) - K(\zeta_2, z)\right) \\
& + \frac{1}{2\pi}\int_{\xi_2}^{\xi_1} K(w, z)Y_L'(w)\mathrm{d}w \\
& + \frac{1}{2\pi}\int_{C_1} \frac{K(w, z)Y_L'(w)}{1 - \mathrm{e}^{-\mathrm{i}LY_L(w)}}\,\mathrm{d}w + \frac{1}{2\pi}\int_{C_2} \frac{K(w, z)Y_L'(w)}{\mathrm{e}^{\mathrm{i}LY_L(w)} - 1}\,\mathrm{d}w. \tag{8.14}
\end{aligned}
$$

Here, $\zeta_1 = z_{L-1}$ is the isolated root and ζ_2 corresponds to the position of the hole. The contribution due to the latter needs to be subtracted in order to cancel the contribution

arising from the integral. The values of ζ_1, ζ_2 as well as the endpoints ξ_1 and ξ_2 of the curve are determined self-consistently by the "boundary conditions"

$$Y_L(\xi_2) = -\pi + \frac{\pi}{L}, \qquad Y_L(\xi_1) = \pi - \frac{\pi}{L},$$
$$Y_L(\zeta_1) = \pi, \qquad Y_L(\zeta_2) = \pi - \frac{4\pi}{L}. \tag{8.15}$$

Assuming an expansion of the form

$$Y_L(z) = \sum_{n=0}^{\infty} L^{-n} y_n(z), \tag{8.16}$$

we can utilize the results of Section 6. If we furthermore assume that ζ_1^{-1} lies inside the contour of integration, we find that $y_0(z)$ is again given by (6.7) and obtain the following result for $y_1(z)$

$$
\begin{aligned}
y_1(z) = &-\mathrm{i}\ln\left[-\frac{z}{z_\mathrm{c}}\frac{1-z_\mathrm{c}^2}{1-z^2}\left(\frac{z_\mathrm{c}-z_\mathrm{c}^{-1}}{z-z_\mathrm{c}^{-1}}\right)^{-\mathrm{i}\lambda_1}\frac{z+a}{z_\mathrm{c}+a}\frac{z+b}{z_\mathrm{c}+b}\right]\\
&-\mathrm{i}\ln\left[\frac{z-1/\zeta_1}{z_\mathrm{c}-1/\zeta_1}\frac{z-\zeta_1}{z_\mathrm{c}-\zeta_1}\right]+\mathrm{i}\ln\left[-\frac{z-1/\zeta_2}{z_\mathrm{c}-1/\zeta_2}\right]\\
&+\kappa_1-\mathrm{i}\ln\left(-\zeta_2ab(-z_\mathrm{c})^{-\mathrm{i}\lambda_1}\right).
\end{aligned}
\tag{8.17}
$$

It is important to note, that expression (8.17) has been derived under the assumption that z^{-1} lies outside the contour of integration[+]. Hence, we cannot use (8.17) to determine ζ_1 via (8.15). However, it turns out that (8.17) already contains sufficient information for determining the leading order of $\mathcal{E}_\mathrm{c}$.

Using the definitions of the points ξ_1, ξ_2 and ζ_2 above, the expansion (6.2) and Appendix B, we find that the intersect of the solution curve with the negative real axis in the limit $L \to \infty$ is now given by

$$z_\mathrm{c} = -(ab)^{-1/4}. \tag{8.18}$$

The $\mathcal{O}(1)$ term of the eigenvalue corresponding to the choice (8.12) is real

$$\mathcal{E}_\mathrm{c}(L) = -\alpha - \beta - \frac{1+3z_\mathrm{c}}{1-z_\mathrm{c}} + o(1), \tag{8.19}$$

where z_c given in (8.18). The subleading corrections are complex. However, the $\mathcal{O}(1)$ contribution (8.19) to the eigenvalue does *not* vanish on the coexistence line. Hence this excitation does not play an important role at large times. We have checked that for $\alpha = \beta = 0.3$ both (8.18) and (8.19) agree well with a direct numerical solution of the Bethe ansatz equations. Based on the above analysis, we conjecture that for all gapless excitations on the coexistence line with eigenvalues that scale with system size as

$$\mathcal{E} = -eL^{-2} + \mathcal{O}(L^{-3}), \tag{8.20}$$

the coefficients e are real. In other words, the dominant large-time relaxation on the coexistence line does not have oscillatory modes.

[+] Otherwise the term $\ln(1 - wz)$ in the kernel $K(w, z)$ would produce an additional contribution in the integro-differential equation for $y_1(z)$.

8.3. Maximum Current phase

Comparing again the numerical solutions of the Bethe ansatz equations to a direct numerical determination of the eigenvalues of the transition matrix for small system sizes L we find that the lowest excitations with non-vanishing imaginary part are characterized by the set of integers

$$I_j = -L/2 + j \quad \text{for} \quad j = 1, \ldots, L-2 \qquad I_{L-1} = L/2, \qquad (8.21)$$

or

$$I_j = -L/2 + j \quad \text{for} \quad j = 2, \ldots, L-1 \qquad I_1 = -L/2. \qquad (8.22)$$

For the first choice the imaginary part of the eigenvalue is positive, whereas the second yields the complex conjugate eigenvalue. In contrast to the corresponding excitations in the massive phase M_I, we find that the gaps in the MC phase remain complex for all values of L.

We denote the complex eigenvalue corresponding to (8.21) by $\mathcal{E}_\mathrm{c}(L)$. We have determined $\mathcal{E}_\mathrm{c}(L)$ from a numerical solution of the Bethe ansatz equations for lattices of up to $L = 1200$ sites and find its leading large L behaviour to be independent of the rates α and β. In what follows we therefore fix $\alpha = \beta = 0.7$, in the understanding that the results for the large-L asymptotics of the eigenvalue of M are universal throughout the maximum current phase.

The distribution of reciprocal Bethe roots for $L = 400$ and $\alpha = \beta = 0.7$ is shown in Figure 12. We observe that the root distribution is quite similar to that of the second lowest eigenvalue in Figure 3. The main difference is that now there is a slight gap between the last two roots.
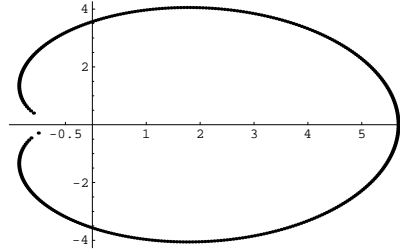

Figure 12. Reciprocal root distributions corresponding to the lowest complex eigenvalue $\mathcal{E}_\mathrm{c}(L)$ for $\alpha = \beta = 0.7$ and $L = 2n = 400$.

Based on the similarity of the root distribution to the one of the lowest excited state, we expect that both real and imaginary parts of $\mathcal{E}_\mathrm{c}(L)$ will be proportional to $L^{-3/2}$ for large systems. This is indeed the case, as is shown in Figure 13, where $\mathrm{Re}(\mathcal{E}_\mathrm{c}(L))$ and $\mathrm{Im}(\mathcal{E}_\mathrm{c}(L))$ are plotted as functions of L^{-1} on a double logarithmic scale for $\alpha = \beta = 0.7$. Both curves are very close to straight lines with slope $3/2$.

In order to determine the asymptotic form of $\mathcal{E}_\mathrm{c}(L)$ more accurately, we repeat the analysis we employed for the lowest excited state in the maximum current phase in section 7. We group the data points for $\mathcal{E}_\mathrm{c}(L)$ in bins containing 11 points each and within each bin perform least square fits to

$$\mathrm{Re}(\mathcal{E}_\mathrm{c}(L)) \approx \mathrm{Re}(e_k) L^{-s_k} \ ,$$
$$\mathrm{Im}(\mathcal{E}_\mathrm{c}(L)) \approx \mathrm{Im}(e_k) L^{-t_k} \ , \quad 20k \leq L \leq 20(k+1). \qquad (8.23)$$
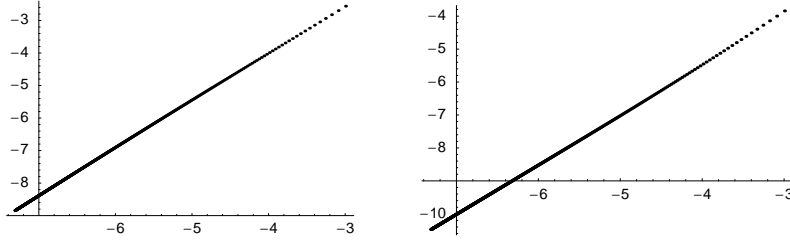
Figure 13. Double logarithmic plots of the real and imaginary parts $\mathcal{E}_{\mathrm{c}}$ as functions of $1/L$.

The resulting sequences of exponents s_k and t_k in the range $30 \leq k \leq 59$ are well approximated by the polynomials

$$s_k \approx 1.4997697 - 0.737888549 k^{-1} + 3.369432984 k^{-2} \,,$$
$$t_k \approx 1.4991041 - 0.423377041 k^{-1} + 6.133640280 k^{-2}. \tag{8.24}$$

The extrapolated values at $k = \infty$ are very close to $3/2$. The fits to the data as well as the extrapolation to $k = \infty$ are show in Figure 14.
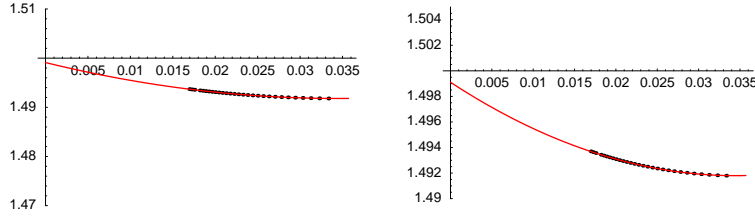
Figure 14. Fits to the exponents s_k and t_k in (8.23) of the real and imaginary parts of $\mathcal{E}_{\mathrm{c}}(L)$ plotted against $1/k$ for $\alpha = \beta = 0.7$.

In order to determine the coefficients of the $\mathcal{O}(L^{-3/2})$ terms, we carry out least square fits of the binned data for $\mathcal{E}_{\mathrm{c}}(L)$ to

$$\mathcal{E}_{\mathrm{c}}(L) \approx -e_k L^{-3/2} - f_k L^{-5/2} \,, \quad 20k \leq L \leq 20(k+1). \tag{8.25}$$

The resulting sequence of coefficients e_k is well described by the polynomial fits (see Figure 15)

$$\mathrm{Re}(e_k) \approx 8.4687424 - 0.1886671 k^{-1} - 12.277915 k^{-2},$$
$$\mathrm{Im}(e_k) \approx -1.6508588 + 0.1263865 k^{-1} + 3.6333854 k^{-2}. \tag{8.26}$$

Extrapolation to the limit $k \to \infty$ then gives the following result for the energy of the first complex excited state of the TASEP in the MC phase

$$\mathcal{E}_{\mathrm{c}}(L) \approx -(8.47 - 1.65\,\mathrm{i})\,L^{-3/2} + \mathcal{O}(L^{-5/2}). \tag{8.27}$$

The result (8.27) can be compared to excited states with complex eigenvalues in the half-filled * TASEP on a ring. We are not aware of any explicit results in the literature

---

* It is natural to compare the the half-filled case, as the average bulk density of the TASEP with open boundaries in the maximum current phase is $1/2$.
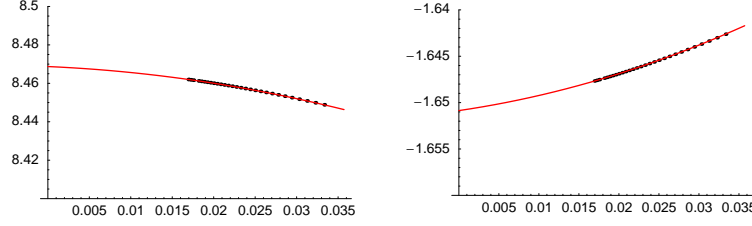
Figure 15. Polynomial fits to the real and imaginary parts of the coefficient e_k in (8.25) plotted against $1/k$ for $\alpha = \beta = 0.7$.

on complex eigenvalues, but they can be easily determined by employing the method of [64]. We summarize some results in (Appendix D). The lowest excited state with complex eigenvalue found to be

$$\mathcal{E}_{\mathrm{c,ring}}(L) \sim -(17.1884\ldots - 5.43662\ldots \mathrm{i})\, L^{-3/2}. \tag{8.28}$$

9. Summary and Conclusions

In this work we have used Bethe's ansatz to diagonalize the transition matrix M for arbitrary values of the rates p, q, α, β, γ and δ that characterize the most general PASEP with open boundaries. The resulting Bethe ansatz equations (3.1), (3.2) describe the *complete* excitation spectrum of M.

We have carried out detailed analyses of the Bethe ansatz equations for the limiting cases of symmetric and totally asymmetric exclusion and determined the exact asymptotic behaviour of the spectral gap for large lattice lengths L. This gap determines the long time $(t \gg L)$ dynamical behaviour of the TASEP. We emphasize that care has to be taken regarding time scales, and that our results below are not valid at intermediate times where the system behaves as for periodic boundary conditions [4].
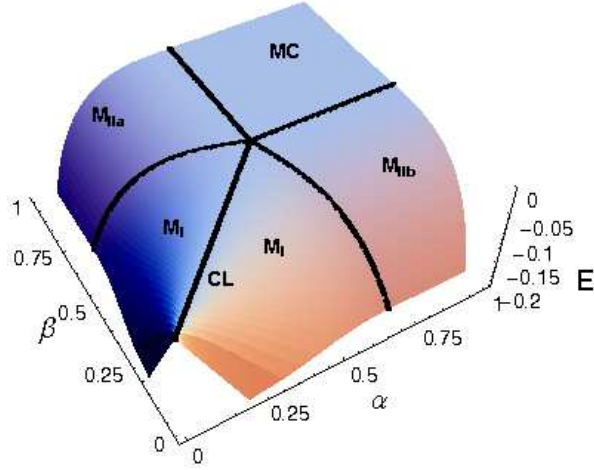
9.1. Dynamical phase diagram

In the case of totally asymmetric exclusion and $\gamma = \delta = 0$, we found that there are three regions in parameter space where the spectral gap is finite and the stationary state is approached exponentially fast. In addition there is one region (maximum current phase) and a line (coexistence line) where the gap vanishes as $L \to \infty$. The resulting dynamical phase diagram ♯ is shown in Figure 16.

Recalling that

$$\beta_{\mathrm{c}} = \left[1 + \left(\frac{\alpha}{1-\alpha}\right)^{1/3}\right]^{-1}, \qquad \alpha_{\mathrm{c}} = \left[1 + \left(\frac{\beta}{1-\beta}\right)^{1/3}\right]^{-1}, \quad (9.1)$$

the leading asymptotic values of the spectral gap in the various regions of the phase diagram of the TASEP are as follows:

♯ We use the term "phase" to indicate a region in parameter space characterised by a particular type of relaxational behaviour.

Figure 16. Dynamic phase diagram determined by the first eigenvalue gap of the TASEP. M_I, M_{IIa} and M_{IIb} are massive phases, CL denotes the critical coexistence line and MC the critical maximal current phase.

Massive Phase M_I: $\alpha < \alpha_c$, $\beta < \beta_c$, $\alpha \neq \beta$

$$\mathcal{E}_1(L) = -\alpha - \beta + \frac{2}{1 + \sqrt{(1-\alpha)(1-\beta)/\alpha\beta}} + \mathcal{O}(L^{-2}). \qquad (9.2)$$

The spectral gap does not vanish as $L \to \infty$, which implies a finite correlation length and an exponentially fast approach to stationarity.

High-Density Phase M_{IIb}: $\beta < 1/2$, $\alpha_c < \alpha$

$$\mathcal{E}_1(L) = -\alpha_c - \beta + \frac{2}{1 + \left[(1-\beta)/\beta\right]^{1/3}} + \mathcal{O}(L^{-2}). \qquad (9.3)$$

The spectral gap is finite and independent of β. The relaxational behaviour is again exponentially fast.

The gap in the low-density phase M_{IIa}: $\alpha < 1/2$, $\beta_c < \beta$ is obtained by the exchange $\alpha \leftrightarrow \beta$. We note that the subdivision of the massive high and low density phases into M_I and $M_{IIa,b}$ is different from the one suggested on the basis of stationary state properties in [16].

Coexistence Line (CL): $\beta = \alpha < 1/2$.

$$\mathcal{E}_1(L) = -\frac{\pi^2 \alpha(1-\alpha)}{1 - 2\alpha} L^{-2} + \mathcal{O}(L^{-3}). \qquad (9.4)$$

The gap vanishes like L^{-2} for large systems, which corresponds to a dynamic exponent $z = 2$ and indicates relaxational behaviour of a diffusive type.

Maximal Current Phase (MC): $\alpha, \beta > 1/2$.

$$\mathcal{E}_1(L) \approx -3.578 L^{-3/2} + \mathcal{O}(L^{-5/2}). \qquad (9.5)$$

Here the gap is independent of the rates α and β. The dynamic exponent $z = 3/2$ is indicative of KPZ like behaviour [5]. We find that the magnitude of $\mathcal{E}_1(L)$ is smaller than half that of the lowest excited state for the TASEP with periodic boundary conditions

$$\mathcal{E}_{1,\mathrm{ring}}(L) \sim -6.50919\ldots L^{-3/2}. \tag{9.6}$$

The two gaps do not seem to be related in any obvious way.

It is known [17] that by varying the bulk hopping rates one can induce a crossover between a diffusive Edwards-Wilkinson (EW) scaling regime [18] with dynamic exponent $z = 2$ and a KPZ regime [5] with $z = 3/2$. Here we have shown using exact methods that a crossover between phases with $z = 2$ and $z = 3/2$ occurs in the case where the bulk transition rates are kept constant, but the boundary injection/extraction rates are varied.

9.2. Domain wall theory

As shown in [29, 30] the diffusive relaxation ($z = 2$) is of a different nature than in the EW regime and is in fact due to the unbiased random walk behaviour of a shock (domain wall between a low and high density region) with right and left hopping rates given by

$$D^{\pm} = \frac{J^{\pm}}{\rho^+ - \rho^-}. \tag{9.7}$$

Here, $\rho^- = \alpha$ and $\rho^+ = 1 - \beta$ are the stationary bulk densities in the low- and high-density phases respectively, and the corresponding currents are given by $J^{\pm} = \rho^{\pm}(1 - \rho^{\pm})$. Our results (9.2) and (9.4) for the massive phase M_{I} and the coexistence line agree with the relaxation time calculated in the framework of a domain wall theory (DWT) model in [30]. This is in contrast to the massive phases M_{II}, where the exact result (9.3) differs from the DWT prediction of [30]. More precisely, the DWT predicts that the relaxational mechanism in the stationary high-density phase ($\beta < 1/2$, $\alpha > \beta$) for $\alpha < 1/2$ is due to the random walk of a "(0|1)" domain wall between a low and a high density segment. On the other hand, in the high-density phase for $\alpha > 1/2$, the DWT predicts a relaxational mechanism based on so-called "(m|1)" domain walls between a maximum current and a low-density region. Our results for the gap exhibit a change of behaviour at $\alpha = \alpha_{\mathrm{c}}$ rather than at $\alpha = 1/2$. We therefore propose the following modified DWT.

We assume that in the high density phase for large α we can still use the DWT rates as given in (9.7), but with an effective density ρ^-_{eff}. In contrast to [30] we do not take the effective density equal to that of the maximum current phase, $\rho^-_{\mathrm{eff}} = 1/2$, but instead determine it below from using a monotonicity argument. Consider first Figure 17, in which we plot the first gap as a function of $\rho^- = \alpha$ for constant $\beta = 0.3$.

- $\alpha < \beta$

  We are in the low density phase. The gap in the infinite volume is finite in this region, but upon increasing α we are driven towards the coexistence line where the gap vanishes and the relaxation is diffusive. Hence, $\partial \mathcal{E}/\partial \alpha > 0$ in this region.

- $\alpha > \beta$

  We are now in the high density region and we expect the gap to be finite again, decreasing with increasing α. Hence, in this region we should have $\partial \mathcal{E}/\partial \alpha \leq 0$. Initially, this is indeed the observed behaviour of the graph of (9.2), but we

see that at $\alpha = \alpha_{\mathrm{c}}$ the graph of (9.2) has local minimum, where the expected behaviour breaks down.
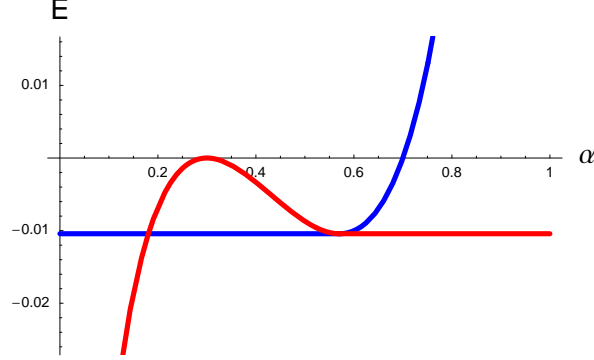
Figure 17. The gap as a function of α for $\beta = 0.3$. The curve corresponds to the function in (9.2) and the horizontal line to (9.3). The gap of the lowest excitation (red online) is a combination of the curve ($0 < \alpha < \alpha_{\mathrm{c}}$) and the line ($\alpha_{\mathrm{c}} < \alpha < 1$).

Hence, for small values of ρ^- and large values of ρ^+ the domain wall theory of [30] correctly predicts the gap to be

$$\mathcal{E}_1(\rho^-, \rho^+) = -D^+ - D^- + 2\sqrt{D^+ D^-}, \tag{9.8}$$

which is equal to (9.2). In the high-density region, there is a critical value $\rho^-_{\mathrm{eff}} = \alpha_{\mathrm{c}}$ beyond which the gap is given by $\mathcal{E}_1(\rho^-_{\mathrm{eff}}, \rho^+)$, where ρ^-_{eff} is determined by

$$\left. \frac{\partial \mathcal{E}_1(\rho^-, \rho^+)}{\partial \rho^-} \right|_{\rho^- = \rho^-_{\mathrm{eff}}} = 0. \tag{9.9}$$

The considerations above are of a sufficiently general nature to remain valid for the wider class of driven diffusive systems that can be described by effective domain wall theories. We emphasize that the DWT as discussed above pertains to the limit $L \to \infty$ only, and that a more careful analysis is necessary to correctly produce the difference in finite size behaviour for the phases M_{I} and M_{II}, see (6.15) and (6.23). In particular, the boundary rates generally need to be chosen differently from the bulk rates. A more detailed comparison of the Bethe ansatz solution and DWT is possible for the case of the PASEP with $Q \neq 0$, where DWT becomes exact for certain values of the rates [65]. This is beyond the scope of the present work and will be discussed in a separate publication [66].

9.3. Higher excitations

Massive Phase M_{I} and Coexistence Line (CL):

The second gap in this phase is given by

$$\mathcal{E}_2(L) = -\alpha - \beta - \frac{2z_{\mathrm{c}}}{1 - z_{\mathrm{c}}} - \frac{4\pi^2}{z_{\mathrm{c}} - z_{\mathrm{c}}^{-1}} \frac{1}{L^2} + \mathcal{O}(L^{-3}), \tag{9.10}$$

where $z_c = -1/\sqrt{ab}$. This result is in agreement with the second gap predicted by the DWT of [30]. In particular, on the coexistence line it corresponds to $n = 2$ of the DWT band of diffusive modes on the coexistence line,

$$\mathcal{E}_n(L) = -\frac{n^2\pi^2}{z_c - z_c^{-1}}\frac{1}{L^2} + \mathcal{O}(L^{-3}). \tag{9.11}$$

The first gap given in (9.4) corresponds to $n = 1$.

We studied the possibility of an oscillating diffusive mode on the coexistence line and found that the first excitation with nonzero imaginary part has a finite gap for $L \to \infty$

$$\mathcal{E}_c(L) = -\alpha - \beta - \frac{1 + 3z_c}{1 - z_c} + o(1), \tag{9.12}$$

where $z_c = -(ab)^{-1/4}$. Although the subleading terms have nonzero imaginary parts, the leading term is real and does *not* vanish on the coexistence line. Hence this excitation does not play an important role at large times. We conjecture that the leading $\mathcal{O}(L^{-2})$ terms of the eigenvalues of all diffusive modes on the coexistence line are real.

Maximum Current Phase MC

We determined the energy of the first "complex" excited state in the MC phase by means of a direct numerical solution of the Bethe ansatz equations. We find it to be independent of α and β and given by

$$\mathcal{E}_c(L) \approx -(8.47 - 1.65\,\mathrm{i})\,L^{-3/2} + \mathcal{O}(L^{-5/2}). \tag{9.13}$$

Complex eigenvalues give rise to interesting oscillations in correlation functions. Such behaviour has been observed for the KPZ equation [67, 68], which is related to the TASEP with periodic boundary conditions. In Appendix D we have computed the low lying complex excitations of the TASEP on the ring using the method of [64]. The lowest such excitation is given by

$$\mathcal{E}_{c,\mathrm{ring}}(L) \sim -(17.1884\ldots - 5.43662\ldots\,\mathrm{i})L^{-3/2}. \tag{9.14}$$

The result (9.14) confirms the prediction from the KPZ equation that both real and imaginary part scale with $L^{-3/2}$ [68]. According to (9.13) this scaling still holds when boundaries are present. However, as was the case with the first gap, although (9.13) does not depend on the boundary rates α and β, its value does not seem to be related to (9.14) in a simple way.

A number of interesting open problems remain. In a forthcoming publication [66] we determine the spectral gaps for the case of partially asymmetric diffusion and $\alpha, \beta, \gamma, \delta \neq 0$ from the Bethe ansatz equations (3.2). As we have discussed, the constraint (1.8) precludes the determination of current fluctuations from the Bethe ansatz. It therefore would be highly desirable to obtain Bethe ansatz equations for the Heisenberg XXZ chain with the most general open boundary conditions. Furthermore, the existing Bethe ansatz solution provides information only about the spectrum, but not the eigenstates of the transition matrix. In order to study correlations functions [39] the knowledge of matrix elements of the spin operators between left and right eigenstates is required. In light of this it would be very interesting to construct the eigenstates from the Bethe ansatz.

Acknowledgments

Appendix A. Analysis of the Abel-Plana Formula

In this appendix we sketch how to extract the finite-size correction terms from the integral expression

$$\mathrm{i}\,Y_L(z) = g(z) + \frac{1}{L}g_{\mathrm{b}}(z) + \frac{1}{2\pi}\int_{\xi^*}^{\xi} K(w,z)Y_L'(w)\,\mathrm{d}w$$

$$+ \frac{1}{2\pi}\int_{C_1} \frac{K(w,z)Y_L'(w)}{1 - \mathrm{e}^{-\mathrm{i}LY_L(w)}}\,\mathrm{d}w + \frac{1}{2\pi}\int_{C_2} \frac{K(w,z)Y_L'(w)}{\mathrm{e}^{\mathrm{i}LY_L(w)} - 1}\,\mathrm{d}w. \quad \text{(A.1)}$$

The main contributions to the correction terms in (A.1) comes from the vicinities of the endpoints ξ, ξ^*. Along the contour C_1 the imaginary part of the counting function is positive, $\mathrm{Im}(Y_L(w)) > 0$, whereas along the contour C_2 it is negative, $\mathrm{Im}(Y_L(w)) < 0$. As a result the integrands decay exponentially with respect to the distance from the endpoints. In the vicinity of ξ, we therefore expand

$$Y_L(w) = Y_L(\xi) + Y_L'(\xi)(w - \xi) + \dots \,. \quad \text{(A.2)}$$

Assuming that $Y_L'(\xi)$ is $\mathcal{O}(1)$ (an assumption that will be checked self-consistently), we find that the leading contribution for large L is given by

$$\frac{1}{2\pi}\int_{C_1} \frac{K(w,z)Y_L'(w)}{1 - \mathrm{e}^{-\mathrm{i}LY_L(w)}}\,\mathrm{d}w \sim \frac{Y_L'(\xi)}{2\pi}\int_{\xi}^{0} \frac{K(w,z)}{1 + \mathrm{e}^{-\mathrm{i}LY_L'(\xi)(w-\xi)}}\,\mathrm{d}w\,,$$

$$- (\xi \to \xi^*). \quad \text{(A.3)}$$

Here we have used the boundary conditions (5.14). Carrying out the analogous analysis for the integral along the contour C_2, we arrive at the following expression for the leading contribution of the last two terms in (A.1)

$$\mathcal{A} = \frac{1}{2\pi}\int_{C_1} \frac{K(w,z)Y_L'(w)}{1 - \mathrm{e}^{-\mathrm{i}LY_L(w)}}\,\mathrm{d}w + \frac{1}{2\pi}\int_{C_2} \frac{K(w,z)Y_L'(w)}{\mathrm{e}^{\mathrm{i}LY_L(w)} - 1}\,\mathrm{d}w$$

$$= \frac{\mathrm{i}}{2\pi L}\int_0^{\infty} \frac{1}{1 + e^x}\left[K\left(\xi + \frac{\mathrm{i}\,x}{LY_L'(\xi)}, z\right) - K\left(\xi - \frac{\mathrm{i}\,x}{LY_L'(\xi)}, z\right)\right]\mathrm{d}x$$

$$- (\xi \to \xi^*). \quad \text{(A.4)}$$

If the endpoints ξ, ξ^* are such that we can Taylor-expand the kernels appearing in (A.4), we can simplify the expression further with the result

$$\mathcal{A} \approx - \frac{K'(\xi,z)}{\pi L^2 Y_L'(\xi)}\int_0^{\infty} \frac{x}{1 + e^x}\,\mathrm{d}x - (\xi \to \xi^*)$$

$$= - \frac{\pi}{12 L^2}\frac{K'(\xi,z)}{Y_L'(\xi)} - (\xi \to \xi^*). \quad \text{(A.5)}$$

This is the leading Euler-MacLaurin correction term that occurs in the low and high density phases, see (6.1). The key in the above derivation was the ability to expand

$$K\left(\xi + \frac{\mathrm{i}\,x}{LY_L'(\xi)}, z\right) - K\left(\xi - \frac{\mathrm{i}\,x}{LY_L'(\xi)}, z\right)$$

$$\sim \ln\left[\frac{LY_L'(\xi)\left(z^{-1} - \xi\right) + \mathrm{i}\,x}{LY_L'(\xi)\left(z^{-1} - \xi\right) - \mathrm{i}\,x}\right] \quad \text{(A.6)}$$

in a power series in x. This is unproblematic as long as $LY_L'(\xi)(z^{-1} - \xi)$ is large, which turns out to be the case in the low and high density phases as well as on the coexistence line.

In the maximum current phase the above analysis no longer holds. As mentioned in the main text, $\xi \to -1$ in the MC phase, and this has two consequences. Firstly, by virtue of the endpoints ξ, ξ^* being close to stationary point, the derivative $Y_L'(\xi)$ is now found to be of order $L^{-1/2}$ whereas $Y_L''(\xi)$ is of order one. As a result (c.f. [25]) we have to retain subleading terms in the Taylor-expansions of $Y_L(w)$ and $Y_L'(w)$ around $w = \xi$, e.g.

$$Y_L(w) \sim Y_L(\xi) + Y_L'(\xi)(w - \xi) + \frac{1}{2}Y_L''(\xi)(w - \xi)^2. \tag{A.7}$$

Secondly, and more seriously, as $\xi - \xi^{-1} = \mathcal{O}(L^{1/2})$ the Taylor expansion of the integration kernel $K(\xi, z)$ breaks down near $z = \xi$. Taking (A.7) into account and following through the same steps as before, we find that the leading contributions of the last two terms in (A.1) in the maximum current phase are

$$\mathcal{A} = \frac{i}{\pi L} \int_0^\infty \frac{x + p}{1 + \exp(x^2 + 2xp)} K\left(\xi + \varepsilon x, z\right)$$

$$- \frac{i}{\pi L} \int_0^\infty \frac{x - ip}{1 + \exp(x^2 - 2ipx)} K\left(\xi + i\varepsilon x, z\right) - (\xi \to \xi^*). \tag{A.8}$$

Here we have introduced

$$\varepsilon = \sqrt{\frac{2i}{LY_L''(\xi)}} = \mathcal{O}(L^{-1/2}), \qquad p = -\frac{i}{2}\varepsilon Y_L'(\xi)L = \mathcal{O}(1). \tag{A.9}$$

In order to make progress we would like to expand around $x = 0$. However, as $z^{-1} - \xi$ becomes of order $\mathcal{O}(L^{-1/2})$ for z near ξ, all the terms $x^n K^{(n)}(\xi, z)$ in the expansion are of the same order L^0 for $(n \geq 1)$, and we would need to self-consistently determine the full series. The $n = 0$ terms in the Taylor expansion, which are proportional to $\ln(L)L^{-1}$, cancel, and we find that $\mathcal{A} = \mathcal{O}(L^{-1})$.

Appendix B. Expansion coefficients

In the following list we abbreviate $y_n'(z_c)$ by y_n',

$$\kappa_1 = -y_0'\delta_1, \tag{B.1}$$

$$\lambda_1 = y_0'\frac{\eta_1}{\pi}, \tag{B.2}$$

$$\kappa_2 = -y_0'\delta_2 - y_1'\delta_1 - \frac{1}{2}y_0''(\delta_1^2 - \eta_1^2), \tag{B.3}$$

$$\lambda_2 = \frac{1}{\pi}\left(y_0'\eta_2 + y_1'\eta_1 + y_0''\delta_1\eta_1\right), \tag{B.4}$$

$$\mu_2 = y_0'\frac{\delta_1\eta_1}{\pi}, \tag{B.5}$$

$$\kappa_3 = -y_0'\delta_3 - y_1'\delta_2 - y_2'\delta_1 - y_0''(\delta_1\delta_2 - \eta_1\eta_2) - \frac{1}{2}y_1''(\delta_1^2 - \eta_1^2)$$

$$- \frac{1}{6}y_0'''\delta_1(\delta_1^2 - 3\eta_1^2), \tag{B.6}$$

$$\lambda_3 = \frac{1}{\pi}\left(y_0'\eta_3 + y_1'\eta_2 + y_2'\eta_1 + y_0''(\delta_1\eta_2 + \delta_2\eta_1) + \delta_1\eta_1 y_1''\right.$$

$$+ \frac{1}{6} y_0''' \eta_1 (3\delta_1^2 - \eta_1^2) \Bigg), \tag{B.7}$$

$$\mu_3 = \frac{1}{\pi} \Bigg(y_0'(\delta_1 \eta_2 + \delta_2 \eta_1) + y_1' \delta_1 \eta_1 + \frac{1}{3} y_0'' \eta_1 (3\delta_1^2 - \eta_1^2)$$

$$+ \frac{\pi^2}{3} \frac{y_0''}{y_0'^2} \eta_1 \Bigg), \tag{B.8}$$

$$\nu_3 = \frac{1}{6\pi} \Bigg(y_0' \eta_1 (3\delta_1^2 - \eta_1^2) - 2\pi^2 \frac{\eta_1}{y_0'} \Bigg). \tag{B.9}$$

## Appendix C. Complex/Real excited states and their Bethe root distributions

As mentioned in the main text, excited states can change from complex- to real-valued with increasing lattice length. In order to illustrate this point we consider the TASEP with $\alpha = \beta = 0.25$. In Fig. C1 we plot the real parts of the eigenvalues of the transition matrix for lattice lengths $L = 4, 5, \ldots, 9$, computed by direct diagonalisation. The lowest excitation always corresponds to a real eigenvalue. For $L = 4, 5, 6$ the excited states with second largest real part are a pair of complex conjugated eigenvalues. For larger L however, this pair becomes a pair of real eigenvalues. In terms of the Bethe roots this comes about in the following way. The pair of complex conjugated eigenvalues corresponds to distributions of integers

$$I_j = -L/2 + j \quad \text{for} \quad j = 1, \ldots, L - 2 \qquad I_{L-1} = L/2, \tag{C.1}$$

and

$$I_j = -L/2 + j \quad \text{for} \quad j = 2, \ldots, L - 1 \qquad I_1 = -L/2, \tag{C.2}$$

respectively. The numerical values of the corresponding Bethe roots for even L are listed in Table C1. When the lattice length exceeds $L = 6$ the nature of the excited states changes. Now there are two *real* eigenvalues corresponding to the distribution (C.2) of integers, see Table C1 for the $L = 8$ site system. Analogous violations of the one-to-one correspondence between sets of integers and roots of the Bethe ansatz equations have been previously observed in both "ferromagnetic" [69] and "antiferromagnetic" [70] situations.
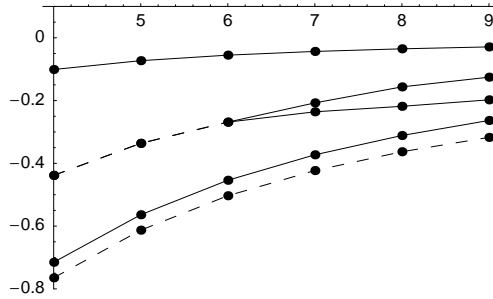
Figure C1. Real parts of the eigenvalues of low-lying excited states for small system sizes $L = 4, 5, \ldots, 9$. The lines are a guide to the eye only. Dashed lines indicate complex conjugate pairs of eigenvalues, solid lines correspond to real eigenavlues.

L	E	integer	root
4	$-0.438276 + 0.118338i$	2	$z_1 = -0.538337 + 0.536475i$
		0	$z_2 = 0.212018 + 0.064141i$
		-1	$z_3 = 0.199931 - 0.122095i$
4	$-0.438276 - 0.118338i$	-2	$z_1 = -0.538337 - 0.536475i$
		0	$z_2 = 0.212018 - 0.064141i$
		1	$z_3 = 0.199931 + 0.122095i$
6	$-0.268648 + 0.037915i$	3	$z_1 = -0.737950 + 0.284318i$
		1	$z_2 = 0.145219 + 0.179042i$
		0	$z_3 = 0.193853 + 0.050586i$
		-1	$z_4 = 0.190087 - 0.072453i$
		-2	$z_5 = 0.130508 - 0.204632i$
6	$-0.268648 - 0.037915i$	-3	$z_1 = -0.737950 - 0.284318i$
		-1	$z_2 = 0.145219 - 0.179042i$
		0	$z_3 = 0.193853 - 0.050586i$
		1	$z_4 = 0.190087 + 0.072453i$
		2	$z_5 = 0.130508 + 0.204632i$
8	-0.156354	4	$z_1 = -0.549451$
		2	$z_2 = 0.062316 + 0.229156i$
		1	$z_3 = 0.141563 + 0.134657i$
		0	$z_4 = 0.173073 + 0.044259i$
		-1	$z_5 = 0.173073 - 0.044259i$
		-2	$z_6 = 0.141563 - 0.134657i$
		-3	$z_7 = 0.062316 - 0.229156i$
8	-0.218262	4	$z_1 = -1.20057$
		2	$z_2 = 0.0876066 + 0.252770i$
		1	$z_3 = 0.163307 + 0.144776i$
		0	$z_4 = 0.193253 + 0.0471657i$
		-1	$z_5 = 0.193253 - 0.0471657i$
		-2	$z_6 = 0.163307 - 0.144776i$
		-3	$z_7 = 0.0876066 - 0.252770i$

Table C1. Low-lying excited states for $\alpha = \beta = 0.25$ and $L = 4, 6, 8$.

Appendix D. Excited States of the TASEP on a Ring

In this appendix we collect some results on the excitation spectrum of the TASEP on a ring, i.e. with periodic boundary conditions. Golinelli and Mallick have recently developed a simple method for calculating the spectral gap in the TASEP on a ring [64]. Their method applies to higher excited states as well. In what follows we consider the case of half-filling only, i.e. $L/2$ particles on a ring with L sites. The Bethe ansatz equations of the half-filled TASEP are [24, 25]

$$(1 - Z_j^2)^{L/2} = -2^L \prod_{k=1}^{L/2} \frac{Z_k - 1}{Z_k + 1}, \quad j = 1, \ldots, \frac{L}{2}. \tag{D.1}$$

$$E = \sum_{j=1}^{L/2} \frac{Z_j - 1}{2}. \tag{D.2}$$

As the right hand side of (D.1) is independent of the index j, we may write [24, 25, 64]

$$(1 - Z_j^2)^{L/2} = -e^{\pi u} , \quad -1 \leq \mathrm{Im}(u) < 1. \tag{D.3}$$

The L roots of this equation are

$$Z_m = -Z_{L/2+m} = \sqrt{1 - y_m} , \quad m = 1, \ldots, \frac{L}{2}, \tag{D.4}$$

where

$$y_m = e^{2\pi(u+\mathrm{i})/L} \, e^{4\pi\mathrm{i}(m-1)/L}. \tag{D.5}$$

The y_m's lie on a circle with radius $e^{2\pi u/L}$ such that

$$0 \leq \arg(y_1) < \arg(y_2) < \ldots < \arg(y_{L/2}) < 2\pi . \tag{D.6}$$

In order to construct a particular solution of the Bethe ansatz equations, one chooses a sequence of roots $y_{c(1)}, \ldots, y_{c(L/2)}$ where $1 \leq c(1) < \ldots < c(n) \leq L$ and then determines the parameter u self-consistently from

$$e^{\pi u} = 2^L \prod_{k=1}^{L/2} \frac{Z_{c(k)} - 1}{Z_{c(k)} + 1}. \tag{D.7}$$

Appendix D.1. Ground State

The ground state of the TASEP on a ring is obtained by choosing $c(j) = j$, $j = 1, \ldots, L/2$. The corresponding distribution of roots y_m is shown in Figure D1.
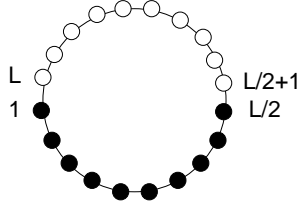
Figure D1. Distribution of roots y_m corresponding to the ground state of the TASEP on a ring.
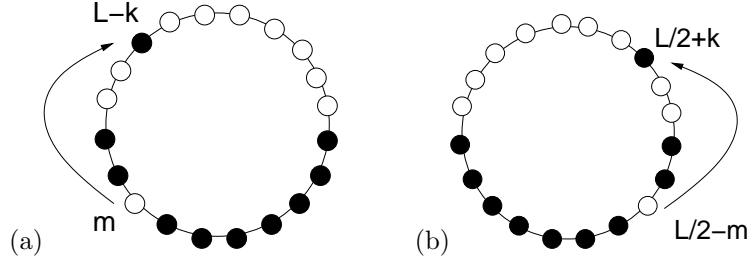
Appendix D.2. Particle-Hole Excitations

Some simple excited states can be constructed by choosing sequences of the type

$$c(j) = \begin{cases} j & \text{if } j < m \\ j+1 & \text{if } m \leq j < \frac{L}{2} \\ L - k & \text{if } j = \frac{L}{2}. \end{cases} \tag{D.8}$$

Such excitations correspond to having a hole at y_m and an extra particle at y_{L-k} as compared to the ground state. The roots distribution is shown in Figure D2(a). In what follows we are interested in the limit $L \to \infty$, while keeping k and m fixed.

Golinelli and Mallick [64] have shown how to simplify and solve the self-consistency condition (D.7) in the large-L limit for the first excited state, which corresponds to the choice $(m, k) = (1, 0)$ in (D.8). Following through exactly the

Figure D2. Particle-hole excitations with energies (a) $E_{m,L-k}$ and (b) $E_{L/2-m,L/2+k}$.

same steps for general (m,k), we obtain the following self-consistency condition for the parameter u in the limit $L \to \infty$

$$\mathrm{Li}_{3/2}\left(-e^{\pi u}\right) + 2\pi \left[\sqrt{-u - (2m-1)\mathrm{i}} + \sqrt{-u + (2k+1)\mathrm{i}} \right] = 0. \quad (D.9)$$

Once u is known from a numerical solution of (D.9) the leading behaviour of the eigenvalue of the transition matrix can be determined from

$$E_{m,L-k} = a_{m,L-k}(u) \left[\frac{2}{L} \right]^{3/2} + \dots \quad (D.10)$$

$$a_{m,L-k}(u) = \frac{\pi^{3/2}}{6} \left[\left(-u - (2m-1)\mathrm{i}\right)^{3/2} + \left(-u + (2k+1)\mathrm{i}\right)^{3/2} \right]$$
$$- \frac{1}{8\sqrt{\pi}} \mathrm{Li}_{5/2}\left(-e^{\pi u}\right). \quad (D.11)$$

The momentum of the particle-hole excitations is given by

$$P_{m,L-k} = -(m+k)\frac{2\pi}{L}. \quad (D.12)$$

We have solved (D.9) for the first few excited states of this type and list the corresponding values of u and the coefficients $a_{m,L-k}$ that characterize the asymptotic behaviour eigenvalues of the transition matrix in Table D1.

The choices $(m,k) = (2,0)$ and $(m,k) = (1,1)$ give the eigenvalues with maximum real part and non-zero imaginary parts.

A second sequence of simple particle-hole excitations is obtained by the choice of sequence

$$c(j) = \begin{cases} j & \text{if } j < \frac{L}{2} - m \\ j+1 & \text{if } \frac{L}{2} - m \le j < \frac{L}{2} \\ \frac{L}{2} + k & \text{if } j = \frac{L}{2}. \end{cases} \quad (D.13)$$

This corresponds to having a hole at $y_{L/2-m}$ and an extra particle at $y_{L/2+k}$. It is easy to see that energy and momentum of such excitations are given by

$$E_{L/2-m,L/2+k} \equiv E_{k,L-m}, \quad (D.14)$$

$$P_{L/2-m,L/2+k} = (m+k)\frac{2\pi}{L}. \quad (D.15)$$

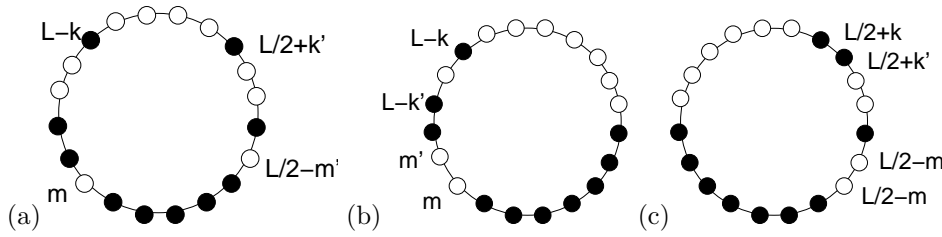| (m,k)	u	$a_{m,L-k}$
$(1,0)$	1.11907	-6.50919
$(2,0)$	$1.55661 - 0.18053\mathrm{i}$	$-17.1884 - 5.43662\mathrm{i}$
$(1,1)$	$1.55661 + 0.18053\mathrm{i}$	$-17.1884 + 5.43662\mathrm{i}$
$(2,1)$	1.90545	-28.9435
$(1,2)$	$1.84895 + 0.313567\mathrm{i}$	$-30.6202 + 14.0523\mathrm{i}$
$(3,0)$	$1.84895 - 0.313567\mathrm{i}$	$-30.6202 - 14.0523\mathrm{i}$
$(2,2)$	$2.15672 + 0.141419\mathrm{i}$	$-43.0859 + 8.57338\mathrm{i}$
$(3,1)$	$2.15672 - 0.141419\mathrm{i}$	$-43.0859 - 8.57338\mathrm{i}$
$(1,3)$	$2.07629 + 0.422166\mathrm{i}$	$-46.2912 + 25.1677\mathrm{i}$
$(4,0)$	$2.07629 - 0.422166\mathrm{i}$	$-46.2912 - 25.1677\mathrm{i}$

Table D1. Eigenvalues of some low-lying excited states for the half-filled TASEP on a ring.

Appendix D.3. Multiple Particle-Hole Excitations

Multiple particle-hole excitations can be constructed along the same lines. We note that while the momentum is additive, i.e. simple the sum of the momenta of the constituent particle-hole excitations, this is not the case for the energy. Hence the Bethe-ansatz particle and holes still interact with one another. Let us first consider a two-particle two-hole excitation characterized by the sequence

$$c(j) = \begin{cases} j & \text{if } j < m \\ j+1 & \text{if } m \le j < \frac{L}{2} - m \\ j+2 & \text{if } \frac{L}{2} - m \le j < \frac{L}{2} - 1 \\ \frac{L}{2} + k' & \text{if } j = \frac{L}{2} - 1 \\ L - k & \text{if } j = \frac{L}{2}. \end{cases} \tag{D.16}$$

This corresponds to having two holes at positions y_m and $y_{L/2-m'}$ and two extra particles at $y_{L/2+k'}$ and y_{L-k}, see Figure Appendix D.3(a).

Figure D3. Two-particle two-hole excitations.

Following once more the procedure of [64] we arrive at the following equation determining the parameter u in the $L \to \infty$ limit

$$\mathrm{Li}_{3/2}\big(-e^{\pi u}\big) + 2\pi\Big[\sqrt{-u - (2m-1)\mathrm{i}} + \sqrt{-u + (2k+1)\mathrm{i}}$$
$$+ \sqrt{-u + (2m'+1)\mathrm{i}} + \sqrt{-u - (2k'-1)\mathrm{i}}\Big] = 0. \tag{D.17}$$

(m, k, m', k')	u	$a_{m,L-k,\frac{L}{2}-m',\frac{L}{2}+k'}(u)$
$(1, 0, 0, 1)$	1.65874	-16.0176
$(1, 1, 0, 1)$	$1.99633 + 0.124903\mathrm{i}$	$-27.8453 + 5.01165\mathrm{i}$
$(2, 0, 0, 1)$	$1.99633 - 0.124903\mathrm{i}$	$-27.8453 - 5.01165\mathrm{i}$
$(1, 0, 1, 1)$	$1.99633 + 0.124903\mathrm{i}$	$-27.8453 + 5.01165\mathrm{i}$
$(1, 0, 0, 2)$	$1.99633 - 0.124903\mathrm{i}$	$-27.8453 - 5.01165\mathrm{i}$
$(2, 0, 0, 2)$	$2.31089 - 0.205544\mathrm{i}$	$-40.3126 - 9.52328\mathrm{i}$
$(1, 1, 1, 1)$	$2.31089 + 0.205544\mathrm{i}$	$-40.3126 + 9.52328\mathrm{i}$
$(2, 0, 1, 1)$	2.29142	-40.4698
$(1, 1, 0, 2)$	2.29142	-40.4698
$(1, 0, 1, 2)$	2.29142	-40.4698
$(2, 1, 0, 1)$	2.29142	-40.4698
$(1, 2, 0, 1)$	$2.23876 + 0.239858\mathrm{i}$	$-42.0218 + 13.3219\mathrm{i}$
$(1, 0, 2, 1)$	$2.23876 + 0.239858\mathrm{i}$	$-42.0218 + 13.3219\mathrm{i}$
$(2, 1, 1, 1)$	$2.57296 + 0.0881572\mathrm{i}$	$-53.6251 + 4.5669\mathrm{i}$
$(1, 1, 1, 2)$	$2.57296 + 0.0881572\mathrm{i}$	$-53.6251 + 4.5669\mathrm{i}$
$(2, 0, 1, 2)$	$2.57296 - 0.0881572\mathrm{i}$	$-53.6251 - 4.5669\mathrm{i}$
$(2, 1, 0, 2)$	$2.57296 - 0.0881572\mathrm{i}$	$-53.6251 - 4.5669\mathrm{i}$

Table D2. Eigenvalues of some low-lying two-particle two-hole excited states for the half-filled TASEP on a ring.

The transition matrix eigenvalue of the two-particle two-hole excitation for very large L is given by

$$E_{m,L-k,L/2-m',L/2+k'} = a_{m,L-k,L/2-m',L/2+k'}(u)\left[\frac{2}{L}\right]^{3/2} + \ldots \quad \text{(D.18)}$$

$$
\begin{aligned}
a_{m,L-k,L/2-m',L/2+k'}(u) = {} & \frac{\pi^{3/2}}{6}\Big\{\big(-u - (2m-1)\mathrm{i}\big)^{3/2} \\
& + \big(-u + (2k+1)\mathrm{i}\big)^{3/2} + \big(-u + (2m'+1)\mathrm{i}\big)^{3/2} \\
& + \big(-u - (2k'-1)\mathrm{i}\big)^{3/2}\Big\} - \frac{1}{8\sqrt{\pi}}\mathrm{Li}_{5/2}\big(-e^{\pi u}\big).
\end{aligned}
\quad \text{(D.19)}
$$

The momentum is equal to

$$P_{m,L-k,L/2-m',L/2+k'} = (m' + k' - m - k)\frac{2\pi}{L}. \quad \text{(D.20)}$$

We have solved (D.17) and (D.19) for some low-lying excited states and list the results in Table D2.

The two-particle two-hole excitations shown in Figures Appendix D.3(b) and (c) can be constructed along the same lines. The transition matrix eigenvalues in the large-L limit fulfil

$$
\begin{aligned}
E_{m,L-k,m',L-k'} &= E_{m,L-k,L/2-k',L/2+m'} \ , \\
E_{L/2-m,L/2+k,L/2-m',L/2+k'} &= E_{k,L-m,L/2-m',L/2+k'} \ .
\end{aligned}
\quad \text{(D.21)}
$$

References

[1] F. Spitzer, Adv. Math. 5, 246 (1970).
[2] T. Liggett, *Interacting Particle Systems*, Springer, New York 1985.
[3] B. Derrida, Phys. Rep. **301**, 65 (1998);
[4] G.M. Schütz, *Phase Transitions and Critical Phenomena* **19** (Academic Press, London, 2000).
[5] M. Kardar, G. Parisi and Y.C. Zhang, Phys. Rev. Lett. **56**, 889 (1986).
[6] B. Schmittmann and R.K.P. Zia, *Statistical Mechanics of Driven Diffusive Systems*, in Phase Transitions and Critical Phenomena Vol 17, eds C. Domb and J.L. Lebowitz, Academic Press, London 1995.
[7] S. Janowsky and J.L. Lebowitz, *Microscopic Models of Macroscopic Shocks*, in Non-equilibrium Statistical Mechanics in One Dimension, ed V. Privman, Cambridge University Press, Cambridge 2000.
[8] K. Hahn, J. Kärger, and V. Kukla, Phys. Rev. Lett. **76**, 2762 (1996).
[9] J.T. MacDonald, J.H. Gibbs and A.C. Pipkin, Biopolymers **6** 1, 1968.
[10] B. Widom, J.L. Viovy and A.D. Défontaines, J. Physique I **1**, 1759 (1991).
[11] G.M. Schütz, Europhys. Lett. **48**, 623 (1999).
[12] D. Chowdhury, L. Santen and A. Schadschneider, Phys. Rep. **329**, 199 (2000).
[13] V. Privman (ed), *Nonequilibrium Statistical Mechanics in One Dimension*, (Cambridge University Press 1997).
[14] J. Krug, Phys. Rev. Lett. **67**, 1882 (1991).
[15] B. Derrida, M. Evans, V. Hakim and V. Pasquier, J. Phys. **A26**, 1493 (1993).
[16] G. Schütz and E. Domany, J. Stat. Phys. **72**, 277 (1993).
[17] J. Neergaard and M. den Nijs, Phys. Rev. Lett. **74**, 730 (1995).
[18] S.F. Edwards and D.R. Wilkinson, Proc. R. Soc. London A **381**, 17 (1982).
[19] S. Sandow, Phys. Rev. E**50**, 2660 (1994).
[20] F.H.L. Essler and V. Rittenberg, J. Phys. **A29**, 3375 (1996).
[21] T. Sasamoto, J. Phys. **A32**, 7109 (1999); J. Phys. Soc. Jpn **69**, 1055 (2000).
[22] R.A. Blythe, M.R. Evans, F. Colaiori and F.H.L. Essler, J. Phys. **A33**, 2313 (2000).
[23] D. Dhar, Phase Transitions **9**, 51 (1987).
[24] L.-H. Gwa and H. Spohn, Phys. Rev. Lett. **68**, 725 (1992); Phys. Rev. A **46**, 844 (1992).
[25] D. Kim, Phys. Rev. E **52**, 3512 (1995).
[26] Z. Nagy, C. Appert and L. Santen, J. Stat. Phys. **109**, 623 (2002).
[27] S. Takesue, T. Mitsudo and H. Hayakawa, Phys. Rev. E **68**, 015103 (2003).
[28] P. Pierobon, A. Parmeggiani, F. von Oppen and E. Frey, Phys. Rev. E**72**, 036123 (2005).
[29] A.B. Kolomeisky, G.M. Schütz, E.B. Kolomeisky and J.P. Straley, J. Phys. **A31**, 6911 (1998).
[30] M. Dudzinski and G.M. Schütz, J.Phys. A **33**, 8351 (2000).
[31] T. Hanney and R.B. Stinchcombe, preprint cond-mat/0606515.
[32] J. de Gier and F.H.L. Essler, Phys. Rev. Lett. **95**, 240601 (2005).
[33] B. Derrida, B. Douçot and P.E. Roche, J. Stat. Phys. **115**, 717 (2004).
[34] B. Derrida, Pramana J. Phys. **64**, 695 (2005).
[35] V. Pasquier, H. Saleur, Nucl. Phys. B **330**, 523 (1990).
[36] J. de Gier, A. Nichols, P. Pyatov and V. Rittenberg, Nucl. Phys. B **729**, 387 (2005).
[37] H.J. deVega and A. Gonzales-Ruiz, J. Phys. **A27**, 6129 (1994).
[38] T. Inami and H. Konno, J. Phys. **A27**, L913 (1994).
[39] V.E. Korepin, A.G. Izergin and N.M. Bogoliubov, *Quantum Inverse Scattering Method, Correlation Functions and Algebraic Bethe Ansatz* (Cambridge University Press, 1993).
[40] J. Cao, H.-Q. Lin, K.-J. Shi, and Y. Wang, Nucl. Phys. **B663**, 487 (2003).
[41] R. I. Nepomechie, J. Stat. Phys. **111**, 1363 (2003); J. Phys. **A37**, 433 (2004);
[42] R. I. Nepomechie and F. Ravanini, J. Phys. **A36**, 11391 (2003).
[43] C. Enaud and B. Derrida, J. Stat. Phys. **114** (2004), 537.
[44] D.J. Evans, E.G.D. Cohen and G.P. Moriss, Phys. Rev. Lett. **71**, 2401 (1993).
[45] G. Gallavotti and E.G.D. Cohen, Phys. Rev. Lett. **74**, 2694 (1995); J. Stat. Phys. **80**, 931 (1995).
[46] J. Kurchan, J. Phys. A **31**, 3719 (1998).
[47] J.L. Lebowitz and H. Spohn, J. Stat. Phys. **95**, 333 (1999).
[48] B. Derrida, B. Doucot and P.-E. Roche, J. Stat. Phys. **115**, 717 (2004).
[49] R.J. Harris, A. Rákos and G.M. Schütz, J. Stat. Mech. (2005) P08003.
[50] J. de Gier and P. Pyatov, J. Stat. Mech.: Theor. Exp. , P03002 (2004).
[51] R. Murgan and R.I. Nepomechie, J. Stat. Mech., P05007 (2005); J. Stat. Mech., P08002 (2005).
[52] W.L. Yang, R.I. Nepomechie and Y.Z. Zhang, Phys. Lett. **B633**, 664 (2006).
[53] R.B. Stinchcombe and G.M. Schütz, Europhys. Lett. **29**, 663 (1995); Phys. Rev. Lett. **75**, 140

(1995).

[54] F.C. Alcaraz, M. Barber, M.T. Batchelor, R.J. Baxter and G.R. Quispel, J. Phys. A**20**, 6397 (1987);

[55] E.K. Sklyanin, J. Phys. A **21**, 2375 (1988).

[56] F.C. Alraraz, M. Droz, M. Henkel and V. Rittenberg, Ann. Phys. (NY) **230**, 250 (1994).

[57] Z. Bajnok, J. Stat. Mech. (2006) P06010.

[58] B. Derrida, E. Domany and D. Mukamel, J. Stat.Phys. **69**, 667 (1992).

[59] C.N. Yang and C.P. Yang, J. Math. Phys. **10**, 1115 (1969).

[60] H.J. de Vega and F. Woynarovich, Nucl. Phys. B **251**, 439 (1985).

[61] F. H. L. Essler, H. Frahm, F. Göhmann, A. Klümper, and V. E. Korepin, *The One-Dimensional Hubbard Model*, Cambridge University Press, Cambridge (2005).

[62] F.W.J. Olver, *Asymptotics and Special Functions*, (AK Peters, Natick MA, 1997).

[63] A.M. Povolotsky, V.B. Priezzhev and C-K. Hu, J. Stat. Phys. **111**, 1149 (2003).

[64] O. Golinelli and K. Mallick, J. Phys. A **37**, 3321 (2004); O. Golinelli and K. Mallick, J. Phys. A **38**, 1419 (2005).

[65] K. Krebs, F.H. Jafarpour and G.M. Schütz, New J. Phys. **5**, 145.1 (2003).

[66] J. de Gier and F.H.L. Essler, unpublished.

[67] F. Colaiori and M.A. Moore, Phys. Rev. Lett. **86**, 3946 (2001); F. Colaiori and M.A. Moore, Phys. Rev. E**65**, 017105 (2002).

[68] M. Prähofer and H. Spohn, J. Stat. Phys. **115**, 255 (2004).

[69] F.H.L. Essler, V.E. Korepin and K. Schoutens, J. Phys. **A25**, 4115 (1992).

[70] F.H.L. Essler, H. Frahm and H. Saleur, Nucl. Phys. **B712**, 513 (1992).